

Modelling conductive thermal transport in three-dimensional fibrous media with fiber-to-fiber contacts

Clémence Gaunand

*Institut Langevin, ESPCI Paris, Université PSL, CNRS - Paris (France),
Saint-Gobain Research Paris - Aubervilliers (France) and
Institut Pprime, CNRS, Université de Poitiers, ISAE-ENSMA - Poitiers (France)*

Yannick De Wilde

Institut Langevin, ESPCI Paris, Université PSL, CNRS - Paris (France),

Adrien François and Veneta Grigorova-Moutiers
Saint-Gobain Research Paris - Aubervilliers (France)

Karl Joulain

Institut Pprime, CNRS, Université de Poitiers, ISAE-ENSMA - Poitiers (France)

(Dated: February 25, 2025)

Understanding heat transfers in fibrous materials, particularly conduction, is a major challenge due to their heterogeneous and multiscale nature, and the unknown contribution of fiber-to-fiber contacts. In most previous modelling studies, the existence of thermal contact resistance is not considered, and the computational complexity often limits the size of simulated samples, which often leads to imprecise or inaccurate predictions. The same problem arises when considering electrical conduction through fibrous materials. In this work, we describe a computationally efficient simulation approach based on multi-nodal representation to analyze the steady-state heat conduction through the solid structure in numerically generated 3D fibrous networks, including contact resistance. We show that the solid conductivity in these networks is governed by a master curve that depends on a single parameter: a characteristic ratio representing the interplay between fiber intrinsic conductivity and contact resistance as well as the influence of other geometric parameters, which numerically validates previous theoretical studies. However, we observe a deviation to this established theory for poorly-connected networks. We derive an expression for a correction factor, considering the influence of correlations between fiber temperatures, and we find then good agreement with our simulation data. Our results demonstrate that the solid conductivity can be fully predicted based on geometric quantities, regardless of the extent of network connectivity, thus generalizing previous studies on this topic. This work, contributing to improve our understanding of conductive heat transport in fibrous media, may prove useful in the development of accurate predictive models and optimization strategies for fibrous insulation materials.

I. INTRODUCTION

Reducing energy costs in the building sector drives important efforts to improve the performance of insulation materials. These materials are generally porous media, in the form of foams or fibrous assemblies. In particular, glasswool, which is composed of glass fibers dispersed in air and linked together by a binder, is one of the most common insulation currently on the market. The thermal performance of an insulation material can be quantified by its effective thermal conductivity k_{eff} . As this quantity refers to a macroscopic scale, it accounts for multiple heat transfer mechanisms: convection, conduction through gas, conduction through the solid phase, and radiation. Improving the efficiency of fibrous insulations requires a quantitative knowledge of these four contributions to heat transport, and more precisely of all the parameters influencing it at the microscale. In media with a pore size below 1 cm, which is the case of glasswool, convection can be neglected [1], leaving only the contributions of conduction and radiation, which can be respec-

tively represented by two independent terms k_{cond} and k_{rad} . Under the hypothesis of low-density, below about $150 \text{ kg}\cdot\text{m}^{-3}$, which is applicable to glasswool, the conductive component can be split as a sum of an air conductivity component $k_{cond,gas}$ and a solid conductivity component $k_{cond,solid}$. This results in the following additive approximation [2]: $k_{eff} = k_{rad} + k_{cond,gas} + k_{cond,solid}$, which means that the three identified contributions to heat transfer are assumed to be uncoupled and can be studied separately. Although many studies have been conducted to quantify the radiative contribution in fibrous materials [3–6], only a few have considered the conduction term and its sensitivity to parameter changes. As the contribution of the gas conductivity can be considered as constant with medium’s density and microstructure, it is interesting to further investigate the impact of conduction through the solid phase in fibrous insulation materials, with the aim of understanding and, subsequently, minimizing this contribution.

As the separate contributions to the effective conductivity cannot be easily measured experimentally, numer-

ical modelling is the preferred tool for their quantitative analysis. The thermal performance of fibrous materials can be investigated numerically using either real structures reconstructed from images, that can be acquired by X-ray tomography [7–9], or virtual samples generated by algorithms [10–12]. The last option enables artificial media to be fitted to real materials using geometric parameters extracted from tomography images, without considering the whole reconstructed 3D structure for the heat transfer calculations, thus improving computational efficiency.

Several methods have previously been proposed to numerically generate a 3D fibrous network. In some studies, fibers are generated so as to directly avoid each other, i.e., they are considered as hard-core objects, which is the most realistic hypothesis from a physical point of view [13–17]. For the sake of simplicity of implementation, soft-core processes, allowing fiber interpenetration, can also be used [18–20]. For example, each fiber can be formed by a chain of spheres with a random walk algorithm: this approach, used by Altendorf and Jeulin [21], can be modified to eliminate fiber overlap [22, 23]. An alternative consists in letting the fibers overlap: this implies making no distinction between intersections and contacts, which is a reasonable assumption when the correlations in the spatial distributions of fibers can be neglected [24, 25].

The case of fibrous insulation materials such as mineral wools has been previously studied by Chapelle et al. [22], Arambakam et al. [26] and Kallel and Joulain [27]. In order to be as representative as possible in terms of network geometry, the authors have chosen a given fiber orientation distribution, first introduced by Schladitz et al. [28] for a stacked fiber system. Among its characteristic is an invariance along the x and y axes, representing the morphology of fibrous insulation materials in relation to their manufacturing process. In these studies, a modified random walk generation method has been used for each fiber, allowing the successive positions of the spheres to be controlled by two parameters so as to create tortuosity.

The volume of the 3D fibrous medium that has to be numerically generated should be set to exceed the representative volume element (RVE), defined as the smallest simulation volume for which the computed properties - in this case the solid conductivity, will be representative of the whole material. This solid conductivity can be numerically computed by different methods. Finite element analysis, used in Refs. [27] and [8], allows a complete representation of the studied structures, resulting in precise yet computationally demanding simulations of the heat transfers, in particular due to the meshing step. An alternative approach to reduce computation time and thus increase the simulation volumes that can be reached is the representation of a fibrous network by a circuit of nodes and branches. This procedure, first used by Kirkpatrick to simulate electrical conductivity [29], is only

applicable to the separate calculation of the contribution of conduction through the solid phase, as opposed to volume averaging methods [30]. Although most studies exploiting this method have applied it to quantifying the solid electrical conductivity of metallic nanotube networks [31–33], very few have extended it to the resolution of thermal transfer problems so far [34].

Independently of the chosen methods for fiber generation and heat transfer calculation in fibrous media, the dependence of thermal or electrical solid conductivity on network parameters has been numerically investigated in various studies [27, 35, 36], only some of which have included the effect of fiber-to-fiber contact resistance [37–40]. It has been found in particular that the Biot number, which compares the conductive thermal resistance in the fiber with the external surface resistance due to thermal losses through contacts [41], has a noticeable impact on the thermal conductivity of fibrous materials [42]. The reported studies have suggested, in some cases, simplified theoretical models [38, 43–45], yet constrained to specific limiting scenarios. Recently, a statistical analysis combined with Fourier’s law has been used to derive a more general theoretical model that predicts the thermal conductivity of dense networks of straight nanofibers, in 2D by Volkov and Zhigilei [46, 47], and in 2D and 3D by Zhao et al. [48]. This theoretical framework generalizes the results of the above-mentioned work by introducing the dependence of solid conductivity on a geometry-dependent resistance ratio. In these studies, the outputs of the model have been exclusively compared with results of numerical simulations in the case of 2D carbon nanotube networks; it is only very recently that Volkov and Zhigilei [49] have presented a first comparison of 3D simulation results, providing at the same time a more accurate theoretical description of semi-dilute systems. However, to the best of our knowledge, there have been no reported studies conducting numerical simulations of 3D networks with variations of all fiber geometric parameters and of contact resistance, making the virtual media representative of a broad spectrum of fibrous materials instead of focusing on an application to metallic nanowires. In particular, anisotropic and poorly-connected 3D systems, which represent the typical case of insulation materials, have not been extensively investigated so far, especially theoretically.

In this work, we focus on quantifying the separate influence of the contribution of conduction through the solid phase to the total heat transfer in fibrous insulation materials, which also includes radiation and conduction through the gas phase. We use a multi-nodal representation to innovatively study the solid conductivity in virtually generated 3D media with straight fibers, with the specific intention to apply the results to the case of real glasswool samples. A methodological advantage of this method is the possibility of directly integrating a fiber-to-fiber contact resistance as an adjustable parameter, while maintaining reasonable computational efficiency.

We demonstrate in particular that the impact of fiber parameters - orientation, length and diameter, as well as that of density, on the conductive properties strongly depends on this contact resistance. More generally, we present a novel approach to quantify the evolution of the solid conductivity in 3D fibrous networks under the form of a master curve, valid regardless of the individual value of these four fiber parameters. We obtain good agreement between our simulation results and the theoretical model introduced by Zhao et al. [48] and Volkov and Zhigilei [46, 47] for high fiber aspect ratios or high fiber volume fractions, and we show that an adaptation of the model is needed in other cases, in accordance with the latest work from Volkov and Zhigilei [49]. A first novelty of our work lies in the validation of this modified theoretical model with simulation data, showing its accuracy for the prediction of the solid conductivity for a wide range of 3D networks including anisotropic and poorly-connected ones, which goes beyond the commonly studied case of metallic nanowires assemblies. Another innovative discovery is the simple formulation of this model depending on geometrical parameters only, revealing in particular the significance of the average number of contacts per fiber as a key parameter governing the extent of the needed correction compared with the initial high-density case. Finally, we have shown a comparison of our simulation and theoretical results, focusing on the specific case of glasswool. This approach gives first insights into the potential impact of contacts on thermal performance at product scale. We also emphasize that our numerical modeling is well suited to predict the electrical conductivity of fibrous media.

This article is organized as follows. In section II A, we explain the fibrous medium generation method used in this work. Then, in section II B, we describe the nodal method used to represent the generated networks by linear circuits and to compute the steady-state heat conduction through the solid phase. Next, numerical results are reported and discussed in section III; the effect of fiber parameters and contact resistance on the evolution of solid conductivity in 3D fibrous networks is analyzed, theoretical considerations are introduced based on simulation results. The final section concludes the paper and outlines interesting research directions for future work.

II. NUMERICAL METHODS

A. Virtual fibrous medium generation

The generated medium is a three-dimensional assembly of straight lines, representing fibers, with an orientation distribution and a prescribed length l . This choice is motivated by the low tortuosity of fibers in glasswool as shown by Optical Coherence Tomography acquisitions, an example of which is provided in Fig. S1 (Supplementary Material) [50]. For each line, one extremity is

randomly placed in a cubic computational domain of side L . Its orientation is defined by a pair of angles (θ_i, φ_i) in spherical coordinates, as shown in Fig. 1(a), sampled according to a directional distribution, the β -orientation distribution, previously used in different modelling studies [21, 22, 26–28].

The azimuthal φ_i angle is chosen from a uniform distribution between 0 and 2π : the density of the distribution is independent of φ , representing the isotropy of the material in the xy -plane. For the choice of the polar angle θ_i , the following marginal probability density function is applied: $g_\beta(\theta) = \frac{\beta \sin \theta}{2[1+(\beta^2-1)\cos^2 \theta]^{3/2}}$, $\theta \in [0, \pi]$, $\beta \in R^+ \setminus \{0\}$. The adjustable parameter β , called the anisotropy parameter, controls the shape and the mean value of the distribution. The case $\beta = 1$ describes an isotropic system; for $\beta \rightarrow 0$, the distribution concentrates around the z -axis and for $\beta \rightarrow \infty$, the orientations are isotropically distributed in the xy -plane. For the sake of convenience, the average polar angle of all fibers $\bar{\theta}$ will be referred to as the network parameter for fiber orientation, rather than β .

Periodic boundary conditions are applied at the lateral edges of the simulation domain, as their use is known to minimize the RVE size [51]. When lines, defined by their starting point and orientation, cross a lateral edge of the domain, they are continued on the opposite side until the prescribed length l is reached. However, this condition is not applied to the lower and upper edges, as they will be connected to different heat baths. This means that a small proportion of lines, those in contact with the lower and upper edges, are stopped before reaching the prescribed length, resulting in an average length slightly inferior to l . In order to guarantee a small difference between these quantities (less than 15%), the condition $L > l$ is applied. It also ensures that no single line is connected to both heat baths at the same time, and that self-interaction between lines due to finite-size effects is limited. In this study, the prescribed length l will be considered as the fiber length, ignoring the small deviation in the mean fiber length that was shown to have a negligible impact on the final results.

The number of lines initially generated in the system is chosen according to a preimposed volume fraction, called the initial volume fraction, and considering them as cylinders with a fixed value d for their diameter. The contacts are then identified using a distance threshold: two lines are considered connected if the smallest distance between them is inferior to their diameter d . In this approximation, the connected fibers are modelled by soft-core, i.e., interpenetrating objects. The soft-core approach does not consider correlations in the spatial distribution of lines, as they may exist in a physical system of connected fibers. However, it has been reported in previous studies [24, 52] that the error introduced by this approximation is small, less than 1% for an aspect ratio $a = l/d \geq 100$, which is the average one in glasswool [53]. It should be noted that lines having less than two contact points cannot be included in the nodal analysis described

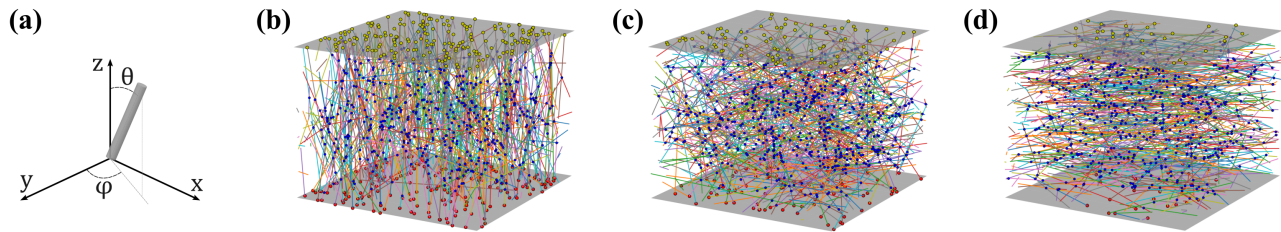


FIG. 1. Examples of generated 3D networks, in which the orientation of one fiber i is described by a polar angle θ_i and an azimuthal angle φ_i in the three-dimensional space (a). In these simulations, $L = 3$ mm, the final volume fraction reached is $V_f = 0.0033$, fiber diameter is $d = 10 \mu\text{m}$, fiber length is $l = 3$ mm and the average polar angle is (b) $\bar{\theta} = 31.8^\circ$ ($\beta = 0.1$), (c) $\bar{\theta} = 57.3^\circ$ ($\beta = 1$), and (d) $\bar{\theta} = 79.9^\circ$ ($\beta = 8$). The yellow (resp. red) circles represent the contact points between a fiber and the upper (resp. lower) edge of the simulation volume, and the blue circles represent the detected contact points between fibers.

in the following, as the resulting thermal network has to be fully connected to be solved by matrix approach. As they do not contribute to heat transfer, after contact detection, these lines are removed from the generated medium, as well as the associated contact points through an iterative procedure. In this study, the volume fraction of the medium V_f is defined as the final one, obtained after fiber removal and therefore inferior to the initial one. Figs. 1(b), (c) and (d) show generated networks using our numerical approach with identification of contact points, for three different angle distributions controlled by the parameter β .

B. Nodal analysis for the resolution of a steady-state conductive heat transport problem

The steady-state conduction through the solid phase in the generated network is computed numerically using the configuration of the guarded hot plate experiment. The upper and lower boundaries of the simulation domain represent two plates with different temperatures, which means that each fiber extremity located at $z = 0$ (resp. $z = L$) will be a temperature source at $T = T_b$ (resp. $T = T_b + \Delta T$), while the fibers will be considered as conductive with an intrinsic thermal conductivity $k_{fib} = 1.3 \text{ Wm}^{-1}\text{K}^{-1}$. This value corresponds to the thermal conductivity of silica glass, the fiber material in glasswool mats. The four other boundaries, on the side of the simulation domain, are assumed to be adiabatic. In the isotropic case, the solid thermal conductivity is the same in each direction. However, if the anisotropy parameter of the distribution orientation is different from unity, the transverse component (i.e., the thermal conductivity in the z direction) differs from the planar component (i.e., that in the x or y directions). This is particularly the case for fibrous insulation materials, due to their layered fiber arrangement [54]. Note that here, in the guarded hot plate experiment configuration, we exclusively simulate the transverse solid thermal

conductivity, referred to in this work as the solid conductivity, meaning the heat flux direction will always be the cross-plane direction for the fibrous medium.

The generated network has to be sufficiently dense or large to reach the RVE and to allow for a low-uncertainty prediction of the solid conductivity. By analogy with an electrical circuit, it can be computed using graph theory, with the Modified Nodal Analysis method [32]. In the steady state, this thermal network is a linear circuit arranged in branches, representing heat flow rates crossing thermal resistances, connected to each other by nodes representing temperatures or temperature sources [34, 55]. This nodal method assumes uniform sections in temperature, i.e., the conductive heat transfer in each fiber will be considered as unidimensional, occurring only in the direction of the fiber. This choice is justified by the average aspect ratio of fibers $a \approx 100$ in glasswool [53]. In particular, the network is modelled using multi-nodal representation, first introduced by Da Rocha et al. [31] for electrical circuits, considering both the internal thermal resistance of fibers and the thermal contact resistance. This modelling method is represented in Fig. 2. In this kind of model, each node represents a contact point: either between a fiber and a temperature source on the upper or lower edge of the simulation cube, or between two fibers. In the latter case, the junction is defined by two distinct nodes linked by an additional branch, that represents the fiber-to-fiber contact resistance. This kind of model differs from the junction resistance-dominated assumption, in which one node represents one fiber, linked by contact resistances, thus ignoring the contribution of the internal resistances. Also, as it can be seen in Fig. 2, when fiber extremities are not touching any other fiber, they are assumed to be adiabatic and therefore are not included in the thermal network.

As the considered heat transfer problem is a steady-state configuration, the associated thermal network can be described by algebraic graph theory. The resolution of a single matrix equation allows to get the vector of tem-

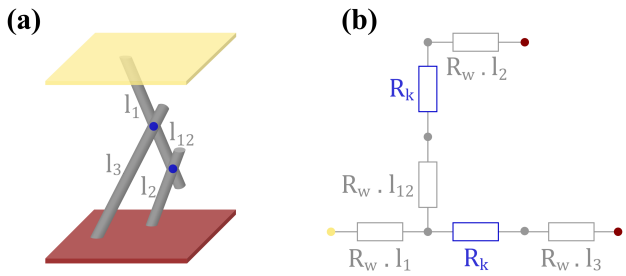


FIG. 2. (a) Simplified network of three connected fibers. Contacts are identified with blue circles. (b) Equivalent thermal circuit of resistances in the steady-state configuration. The dots represent nodes, in particular, yellow and red dots corresponds to temperature sources. A given branch f can be associated with either a contact resistance R_k , or an internal resistance $R_w l_f$ proportional to its length where $R_w = \frac{4}{k_{fib} \pi d^2}$.

peratures and that of heat fluxes, making possible the representation of the temperature field in the network as shown in Fig. 3 for different angle distributions (see Appendix A for details on the resolution method). Then, the total heat flux Q is computed by adding the contributions from the branches in contact with the upper or the lower edge of the simulation domain, and the solid thermal conductivity is calculated by: $k_{cond,solid} = QL/(L^2 \Delta T)$. As the thermal properties of individual fibers, the fiber conductivity k_{fib} and the fiber-to-fiber contact resistance R_k , are assumed to be independent of the temperature, the solid conductivity does not depend on T_b and ΔT .

In order to lower the uncertainty of the simulation results, the selected value of the solid thermal conductivity for a defined set of parameters is the mean of $k_{cond,solid}$ over 5 realizations; its associated 95% confidence interval is also computed and is represented under the form of error bars in all figures shown in this paper. This confidence level is a common choice in statistics: it has been used in particular in previous studies on similar fibrous systems, with $n \approx 10$ realizations [51, 56]. In this present work, errors are calculated using Student's probability distribution, taking into account the fact that the standard deviations of samples of $n = 5$ realizations underestimate the true Gaussian standard deviations. The relative error ϵ_{rel} on $k_{cond,solid}$ for each simulation point is obtained from the following expression: $\epsilon_{rel} = \frac{t_{n-1}(1-\alpha/2)s}{\bar{k}_{cond,solid}\sqrt{n}}$ where α is the significance level: here, $\alpha = 0.05$ to achieve a 95% confidence interval. In this expression, $\bar{k}_{cond,solid}$ is the sample mean, s is the unbiased estimator of the standard deviation given by $s = \sqrt{\frac{\sum_{i=1}^n (k_{cond,solid}^i - \bar{k}_{cond,solid})^2}{n-1}}$, and $t_{n-1}(1-\alpha/2) = 2.78$ is the critical value of the t-distribution for a 95% confidence level. $n - 1$, the number of realizations minus one, represents the number of degrees of freedom, i.e., the number of values that are allowed to vary when estimating the statistic.

For each set of parameters, the sample volume $V = L^3$ is chosen so as to exceed the RVE, on top of the previous condition $L > l$. In this study, the RVE is defined as the volume for which the relative error on the solid thermal conductivity ϵ_{rel} introduced above is smaller than 5% for $R_k = 0$. This relative error criterion has been selected as similar approach was used by Altendorf et al. [51] for the selection of RVE in fibrous media; it also ensures a reasonable computation time. The procedure for selecting L is illustrated in Fig. S2 (Supplementary Material) [50]: starting from a domain size slightly larger than the fiber length, it is gradually increased until the average of $k_{cond,solid}$ for $R_k = 0$ on 5 realizations satisfies the error criteria $\epsilon_{rel} < 5\%$, which also corresponds to achieving convergence of results. This ensures that the simulation results represent the whole network and are not dominated by the behavior of individual fibers. As a consequence of this procedure, the chosen value of L depends on the input parameters; this is represented in Fig. S3 (Supplementary Material) [50]. To reach the RVE, a larger domain size is required when the volume fraction decreases, or when fiber dimensions increase, all other parameters being fixed, which can be attributed to the decrease of the total number of fibers. In contrast, the average fiber angle appears to have only a minor impact on the selection of L .

Numerical simulations are performed to independently study the influence of geometric fiber parameters on the resulting thermal properties of the network. In particular, the joint effects of fiber volume fraction V_f , fiber length l , fiber diameter d and fiber orientation $\bar{\theta}$ with contact resistance R_k are investigated. For each set of parameters and on top of the conditions on V and on L described previously, as some fibers are deleted in the generation process, the orientation and length distributions are compared between the initial and final states, to ensure they are not substantially modified. For all simulations in this study, the size of the calculation domain ranges from $L = 1.25$ mm to $L = 6$ mm depending on the four parameters, the contact density from 40 to 20000 mm⁻³, the average number of contacts per fiber from 2 to 20, and the fiber density from 25 to 4000 mm⁻³.

III. RESULTS AND DISCUSSION

A. Effect of thermal contact resistance on the solid conductivity in relation to fiber properties

1. Effect of thermal contact resistance at different fiber volume fractions

The variation of solid conductivity with fiber volume fraction V_f , fixing fiber orientation, length and diameter, is illustrated in Fig. 4(a) for different contact resistances. Volume fractions between 0.0075 and 0.1 are studied, corresponding to glasswool mat densities ranging from 17 kg.m⁻³ to 221 kg.m⁻³. In all cases, the solid

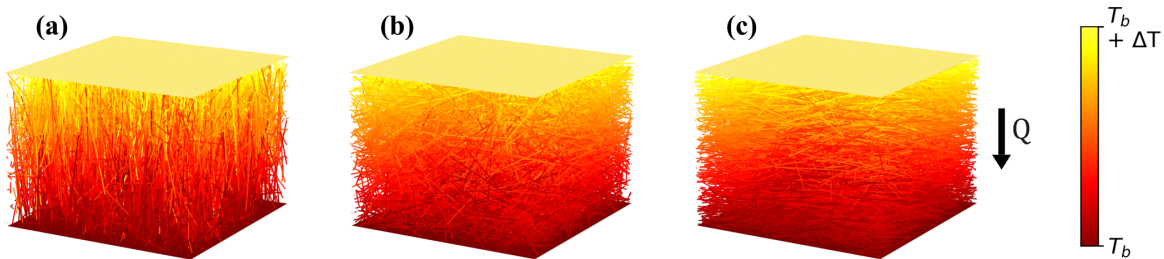


FIG. 3. Temperature field distributions in generated networks with $L = 3$ mm, $V_f = 0.0198$, $l = 2$ mm, $d = 10$ μm and (a) $\bar{\theta} = 31.8^\circ$ ($\beta = 0.1$), (b) $\bar{\theta} = 57.3^\circ$ ($\beta = 1$), and (c) $\bar{\theta} = 79.9^\circ$ ($\beta = 8$), containing between 3720 and 3990 fibers. The upper and lower edges of the simulation domain are areas where the temperature is imposed, generating a heat flux Q in the vertical direction. The angle θ_i of each fiber i is therefore its angle with respect to the direction of heat flux. The coordinate system used is the one represented in Fig. 1(a).

conductivity increases with density in a non-linear way; in particular, it shows power-law behavior at high volume fractions ($V_f \geq 0.03$) indicated by the dashed line best-fits. The graph also shows that the increase in solid conductivity with volume fraction becomes more pronounced as the contact resistance increases, i.e., the exponent in the power law increases, from 1.25 for $R_k = 0$ to 2.23 for 10^9 KW^{-1} . This generalizes previous results reported in Refs. [38] and [40] for 2D networks to the case of 3D networks. These studies have also distinguished two regimes depending on volume fraction: the low-density regime, close to the percolation threshold, exhibits a different behavior from that observed at higher densities. This is presumably due to a difference in the degree of connectivity of the networks, i.e., in the proportion of fibers and contacts conveying heat. Indeed, the contact density increases when the volume fraction increases, as shown in Fig. 4(b). For high densities, it is expected to follow a square power law [38], which is verified in our simulation results for $V_f \geq 0.03$. This value of volume fraction provides a first estimate of the high-density threshold for the chosen simulation parameters, consistent with the validity range of the power laws introduced in Fig. 4(a). According to this estimation, networks with $V_f = 0.01$ should correspond to a low-density regime in which the connectivity is low: to simplify the study of the impact of the other fiber parameters, this value of volume fraction will be chosen in the following sections.

2. Effect of thermal contact resistance at different fiber orientations

Fig. 5(a) illustrates the variation of solid conductivity as a function of the mean angle between the fibers and the heat flux direction $\bar{\theta}$, for different values of contact resistance and for fixed fiber length, diameter and volume fraction. The mean angle $\bar{\theta} = 57.3^\circ$ corresponds to a uniform distribution in spherical coordinates, i.e., to $\beta = 1$; then β is increased up to 30, corresponding to a mean

angle of 85.5° , so as to cover the estimated range for $\bar{\theta}$ in glasswool, between 75° and 85° [53]. For the sake of completeness, we have also included in this figure the simulation results obtained for $\beta < 1$. As β decreases below 1 and approaches 0, fibers become increasingly aligned parallel to the z -axis, as it can be seen in Figs. 1 and 3. Note that this case is not representative of insulation materials, in which fibers tend to form significant angles to the heat flux direction. The graph shows that the solid conductivity decreases as the mean angle to the heat flux direction increases whether contact resistances are integrated or not. This indicates that the impact of contacts on solid conductivity does not change with the orientation of fibers, including when they tend to align with the heat propagation axis.

Note that at sufficiently low densities, the interconnected conduction paths are few in number and can be neglected as a first approximation. In this case, a simplified expression for the total thermal resistance can be built based on simplified networks such as those represented in Fig. 5(b), accounting for the contributions of several conduction paths in parallel, each consisting of several fibers in series. The total resistance R_t of such networks is the ratio of two parameters: the average resistance of the paths R_p and the number of conductive paths in parallel n_p [57, 58]. This average path resistance R_p is the result of two factors that add up as a series: the total resistance of contacts, and the total internal resistance of the path. Therefore,

$$R_t = \frac{1}{n_p} \left(n_{c,p} R_k + \frac{4l_p}{\pi k_{fib} d^2} \right) \quad (1)$$

or

$$R_t = \frac{1}{n_p^2} \left(n_{c,tot} R_k + \frac{4l_{tot}}{\pi k_{fib} d^2} \right) \quad (2)$$

where $n_{c,p}$ is the average number of contacts per path, $n_{c,tot}$ the total number of contacts, l_p the average length of a path and l_{tot} the total length of the paths. In these considerations, the unconnected fiber ends are neglected:

therefore, it is assumed that l_{tot} is the total length of fibers in the networks. As shown in Fig. 5(b), more fibers are needed to connect one heat bath to the other through one path when $\bar{\theta}$ increases. Therefore, the created paths are overall less direct and longer, leading to a decrease in the total number of paths n_p . As the volume fraction and the fiber dimensions are fixed in the simulations, the total fiber length is constant: Eq. (2) confirms that R_t increases with $\bar{\theta}$ when there is no contact resistance, leading to a decrease in the conductivity. Moreover, the parameter governing the relative impact of contacts with respect to that of internal resistance is the total number of contacts $n_{c,tot}$. Fig. 5(c) shows that the volume density

of contacts remains around 200 mm^{-3} regardless of fiber orientation for the simulation parameters chosen in this study: this supports our observation that the effects of contacts and of fiber mean angle on the network are not correlated in the studied range, and particularly in that representative of glasswool.

3. Effect of thermal contact resistance at different fiber lengths

Fig. 6(a) displays a plot of solid conductivity versus fiber length l for different contact resistances, fixing the other fiber parameters. Fiber length ranges from

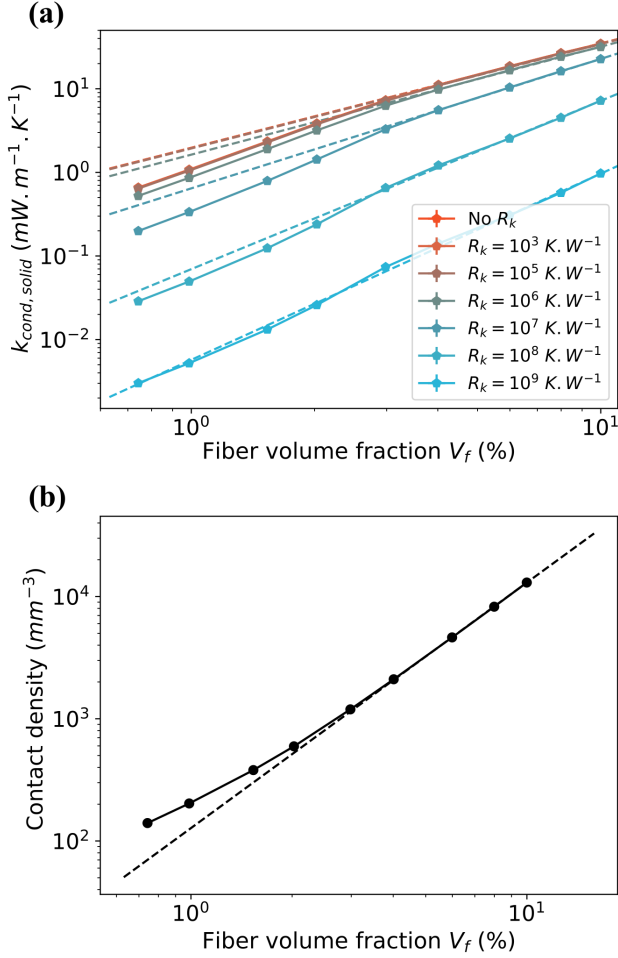


FIG. 4. (a) Solid conductivity as a function of fiber volume fraction for different thermal contact resistances. The dashed lines indicate the power laws best fits to the simulation data for $0.03 \geq V_f \geq 0.1$, with exponents varying ranging from 1.25 to 2.23 as the contact resistance increases from 0 to 10^9 KW^{-1} . The constant input parameters are $l = 1 \text{ mm}$, $d = 10 \mu\text{m}$ and $\bar{\theta} = 57.3^\circ$. (b) Plot of the corresponding contact densities, as a function of fiber volume fraction. The dashed line indicates the square power law best fit to the simulation data for $0.03 \geq V_f \geq 0.1$.

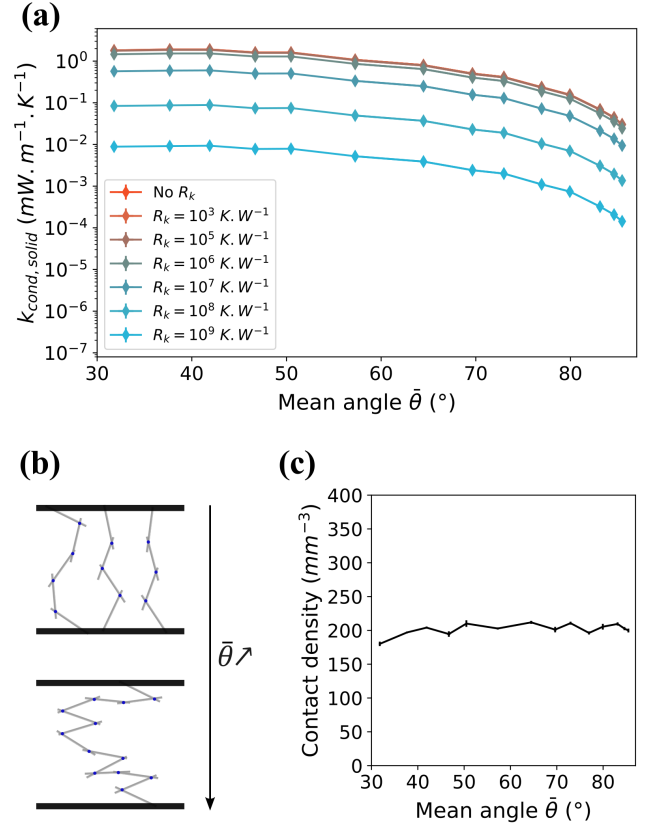


FIG. 5. (a) Solid conductivity as a function of the mean angle to heat flux direction for different thermal contact resistances. The anisotropy parameter β ranges from 0.1 to 30, corresponding to mean angles $\bar{\theta}$ between 31.8° and 85.5° : only data obtained for $\beta > 1$, i.e., for networks in which fibers are preferentially oriented in the cross-plane direction, are representative of insulation materials such as glasswool. The constant input parameters are $l = 1 \text{ mm}$, $d = 10 \mu\text{m}$ and $V_f = 0.01$. (b) Representation of simplified networks illustrating a qualitative argument for the dependence of the conductivity on the mean angle to heat flux direction: when it increases, the number of conduction paths decreases. (c) Plot of contact densities, corresponding to the simulations of (a), as a function of the mean angle.

0.75 mm to 5 mm in the simulations, remaining within the same order of magnitude of 1 mm, which is that representative of glasswool [53]. The graph shows that when no contact resistance is considered, the solid conductivity increases when fiber length increases. Including the impact of junctions between fibers, our results show that an increasing contact resistance induces a decrease in the solid conductivity compared with its value at $R_k = 0$, and that the impact of fiber length is amplified when the contact resistance increases. This means that contact resistance has a lower relative impact for longer fiber assemblies. This behavior is in agreement with the results obtained in Ref. [40] for electrically conducting 2D nanowire networks.

The density and diameter being fixed, the total length is constant and the number of fibers needed to create a path decreases when l increases. Conduction paths are becoming less tortuous and shorter: as a consequence, more conduction paths in parallel can convey heat. Ac-

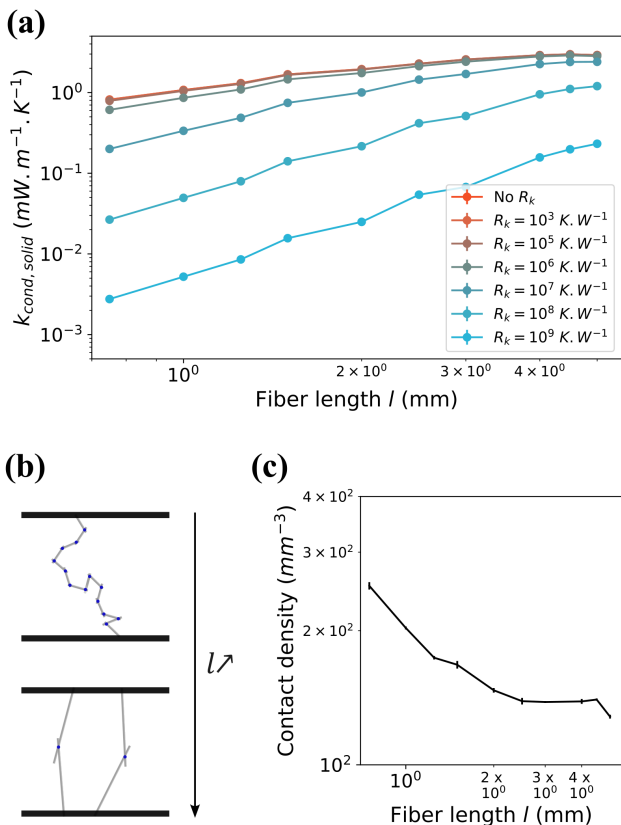


FIG. 6. (a) Solid conductivity as a function of fiber length for different thermal contact resistances. The constant input parameters are $\theta = 57.3^\circ$, $d = 10 \mu m$ and $V_f = 0.01$. (b) Representation of simplified networks illustrating a qualitative argument for the dependence of the conductivity on fiber length: when it increases, the number of conduction paths increases and the number of contacts per path decreases [59]. (c) Plot of contact densities, corresponding to the simulations of (a), as a function of fiber length.

ording to Eq. (2), this explains the observed increase in the solid conductivity when there is no contact resistance; Fig. 6(b) illustrates this situation. Eq. (2) also shows that when it comes to the impact of contacts in simplified networks, the total number of contacts is the parameter that determines its relative importance with respect to the impact of internal resistance, similar to the case of fiber orientation variation. The evolution of contact density versus fiber length is presented in Fig. 6(c). For $l < 2.5$ mm, contact density decreases with fiber length. Then, it seems to reach a threshold - the onset of decline observed at $l > 4.5$ mm remains to be confirmed by further simulations. This behavior is in accordance with previously established theoretical models that estimate the number of contacts in a network of lines [60]. Overall, we find that contact density tends to decrease over the studied range. According to Eq. (2) and as represented in the examples of Fig. 6(b), this should lead to a reduction of the resistive contribution of contacts in the network as there are fewer contacts per path, which is consistent with the correlation observed in Fig. 6(a) between impact of contacts and impact of fiber length.

4. Effect of thermal contact resistance at different fiber diameters

Note that even though widthless sticks are considered in the generation method, a diameter d is taken into account both through the contact detection threshold and the expression of the intrinsic resistance of fibers $R_{fib} = \frac{4l}{k_{fib}\pi d^2}$. Its influence on the solid conductivity for different contact resistances is represented in Fig. 7(a). The diameter ranges from $2 \mu m$ to $20 \mu m$ as so as to cover the sizes of the glass fibers that can be found in real glasswool mats [53]. The graph shows that with no contact resistance, the solid conductivity decreases when fiber diameter increases. Also, similar to the case of fiber length, the impact of fiber diameter is amplified when the contact resistance increases.

Our numerical results indicate that among the four ranges of variation for fiber parameters studied individually, the one chosen for fiber diameter leads to the greatest variation in the total number of fibers. This means that changing the diameter between $2 \mu m$ and $20 \mu m$ greatly affects the connectivity of the network. As a consequence, the assumption of low-density in the sense of no interconnection between conduction paths cannot be made here over the whole diameter range, even though the volume fraction is fixed at 0.01. Networks with a higher diameter are composed of less fibers, and therefore exhibit less connectivity, leading to a less efficient heat flux distribution which explains the observed decrease in the solid conductivity. This effect is expected to be important as the fixed volume fraction is low [61]. Moreover, once again Eqs. (1) or (2) give insights about the evolution of the relative impact of contacts with respect to that of the internal resistance with fiber diameter,

which is illustrated by simplified networks in Fig. 7(b). The total contact density decreases as the fiber diameter increases – this is verified by simulation results shown in Fig. 7(c), and the number of conduction paths in parallel decreases as well. From Eq. (1), assuming constant l_p and $n_{c,p}$, an increase in fiber diameter increases the ratio of the resistive contribution of contacts over that of paths due to its dependence on d^2 . This leads to an amplification of the impact of the remaining contacts resistances, even though there are fewer of them. These considerations, although there are limited to a simplified case with no interconnection, are consistent with the correlation between impact of contacts and impact of fiber diameter observed in Fig. 7(a).

Note that while in this study, contact resistance and

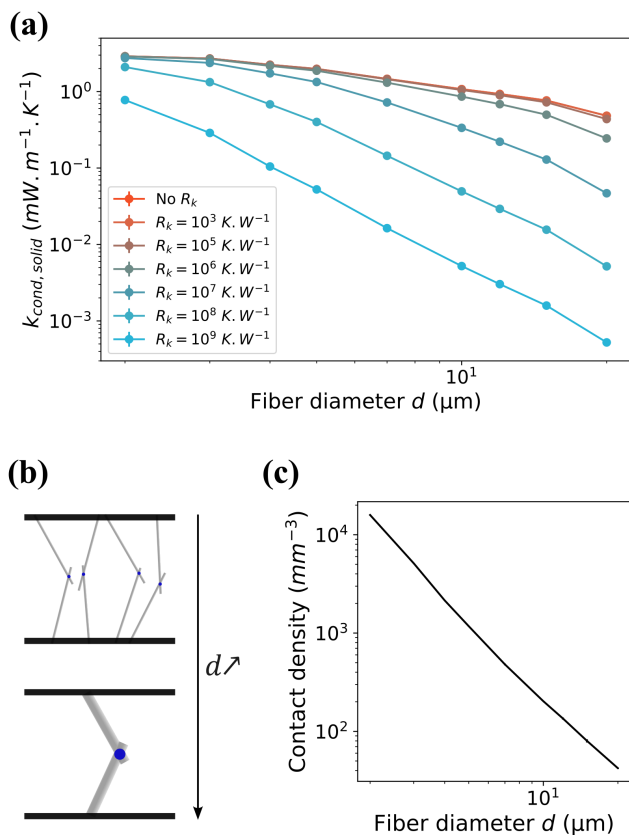


FIG. 7. (a) Solid conductivity as a function of fiber diameter for different thermal contact resistances. The constant input parameters are $\bar{\theta} = 57.3^\circ$, $l = 1$ mm and $V_f = 0.01$. (b) Representation of simplified networks illustrating a qualitative argument for the dependence of conductivity on fiber diameter: when it increases, the number of conduction paths in parallel decreases. Assuming a constant number of contacts per path, the number of contacts resistances R_k in parallel decreases, leading to an increase in the total resistive contribution of junctions, which goes from $R_k/4$ to R_k in this example [59]. (c) Plot of contact densities, corresponding to the simulations of (a), as a function of fiber diameter.

fiber diameter are treated as independent, it is likely that a correlation exists between these two parameters [59]. Indeed, glass fibers are expected to deform at a junction, according to the Hertz contact law. Therefore, the contact area between fibers with a larger diameter would increase, leading to a lower associated contact resistance. In the configuration studied here, that can be described as a perfectly rigid assumption, one can notice that the effects of fiber length and diameter seem to have inverse effects, indicating a potential dependence of the network properties on the aspect ratio a . In particular, the influence of aspect ratio on the solid conductivity is amplified in the case of resistive contacts, which was also reported in Ref. [42].

B. Unified description of the evolution of the solid conductivity

As the conductivity of fibers k_{fib} is fixed in the simulations discussed in the previous section, changing the value of the contact resistance R_k amounts to changing the resistance ratio R_k/R_{fib} where $R_{fib} = \frac{4l}{k_{fib}\pi d^2}$ is the intrinsic resistance of fibers. We verified by additional simulations that modifying the value of R_k/R_{fib} by increasing R_k or decreasing k_{fib} gives the same results, for an identical network structure. Besides the resistance ratio, our results demonstrate that fiber parameters also participate in the control of conduction in the network. A relevant measure of this interplay between the intrinsic and contact resistances that takes into account the network geometry is given by a dimensionless parameter r introduced in a theoretical model by Zhao et al. [48] and Volkov and Zhigilei [46, 49]:

$$r = \frac{2l\langle|\cos\theta|\rangle}{\langle H\rangle\langle N_c\rangle} \frac{R_k}{R_{fib}} = \frac{R_k\langle|\cos\theta|\rangle k_{fib}\pi d^2}{2\langle H\rangle\langle N_c\rangle} \quad (3)$$

where $\langle N_c\rangle$ is the average number of contacts per fiber, $\langle H\rangle$ is the average vertical distance between two centers of fibers in contact, and $\langle|\cos\theta|\rangle$ is the average cosine of the polar angle of fibers. As highlighted by the authors, the theoretical models for 2D and 3D fibrous networks are similar, as a 3D network becomes 2D if the azimuthal angle reaches $\varphi = \pi/2$. Note that this transition from 3D to 2D networks is not investigated in this study as the azimuthal angle is always chosen from a uniform distribution: the distribution of polar angles θ is the only one that can change. According to this model, the solid conductivity in a 3D fibrous network is given by:

$$k_{cond,solid} = \frac{1}{4} k_{fib}\pi d^2 \langle n_z\rangle \langle|\cos\theta|\rangle \frac{1}{1+r} = k_{0,th} \frac{1}{1+r} \quad (4)$$

where $\langle n_z\rangle$ is the average areal number density of fibers through a horizontal section, and $k_{0,th} =$

$\frac{1}{4}k_{fib}\pi d^2\langle n_z \rangle \langle |\cos\theta| \rangle$ is the theoretical value of the conductivity at $R_k = 0$. This model is based on the assumptions of linearity of the temperature distributions along fibers, and of non-correlations between the temperatures of two fibers in contact.

Fig. 8 compares the predictions of Eq. (4) to simulation data collected in this study, for different fiber volume

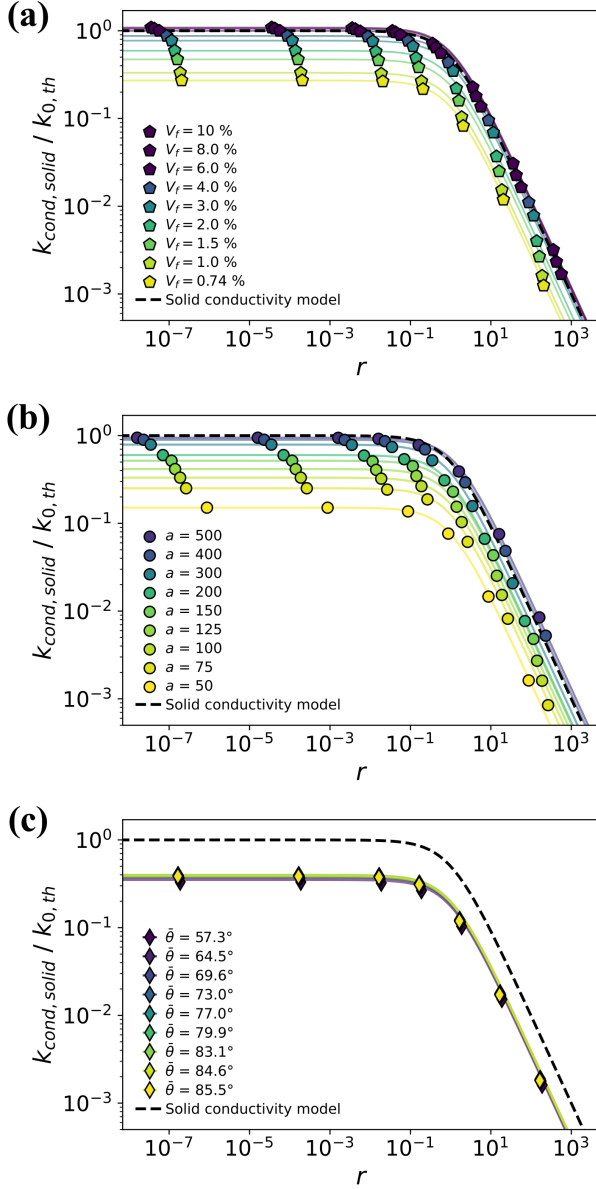


FIG. 8. Solid thermal conductivity normalized to $k_{0, th}$, the theoretical conductivity at $R_k = 0$, as a function of the characteristic dimensionless parameter r , for (a) different volume fractions V_f , (b) different aspect ratios a , and (c) different fiber orientations governed by the mean angle to heat flux direction $\bar{\theta}$. The base parameters are $V_f = 0.01$, $a = 100$ and $\bar{\theta} = 57.3^\circ$. The black dashed line shows the predictions of Eq. (4).

fractions, aspect ratios, and orientations. Note that here, only networks with fiber mean angles between 57° and 86° , i.e., with $\beta > 1$, are considered, which is the only regime representative of real-world insulation materials. Fig. 8(a) indicates that the agreement between simulations and theory is improved when the volume fraction increases, as mentioned above. Similarly, Fig. 8(b) demonstrates a comparable trend concerning the aspect ratio. Note that this parameter has an effect independently of the individual values of l and d and is an important quantity in the conductivity scaling, which is consistent with our previous hypothesis. According to Fig. 8(c), fiber orientation does not have any effect on the relative variation of $k_{cond, solid}$ with r , indicating that the accordance between theory and simulation is fully determined by the values of V_f and a . Overall, Fig. 8 shows that the above theoretical model seems to be relevant for 3D fibrous networks in the case of high volume fractions ($V_f > 0.05$ when $a = 100$) and high aspect ratios ($a > 450$ when $V_f = 0.01$), when adopting representative values of the properties of glasswool for the other parameters.

Fig. 9 represents, for different fiber parameters, the solid conductivity normalized to k_0 , its value at $R_k = 0$, as a function of the characteristic dimensionless parameter r . Simulated data is compared with the prediction $\frac{1}{1+r}$ given by Eq. (4). One can see that all markers corresponding to the simulation data collapse into a single master curve, regardless of the fiber volume fraction, aspect ratio or mean orientation, that is in good agreement with the theoretical model. This comparison validates, for any value of these network parameters, the consideration of r as the characteristic parameter governing the evolution of solid conductivity as the contact resistance (or the intrinsic conductivity of fibers) changes. In the general case of a 3D fibrous assembly represented by

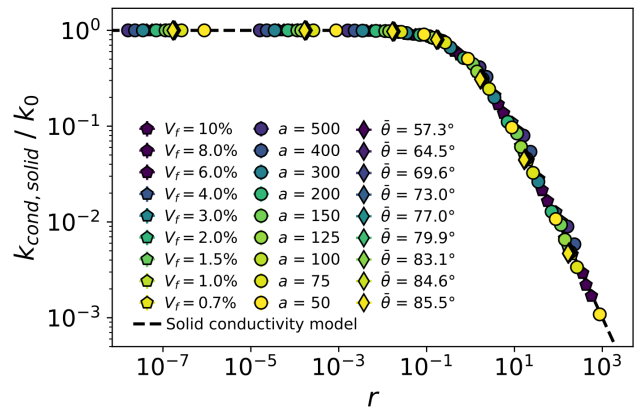


FIG. 9. Solid thermal conductivity normalized to k_0 , the simulated conductivity at $R_k = 0$, as a function of the characteristic dimensionless parameter r , for different volume fractions V_f , aspect ratios a and mean angles $\bar{\theta}$, the base parameters being $V_f = 0.01$, $a = 100$ and $\bar{\theta} = 57.3^\circ$. The black dashed line shows the predictions of Eq. (4).

straight lines, this quantity correctly describes the joint effect of resistance ratio and geometric properties. Obtaining this master curve also indicates that the deviation observed in Fig. 8(a) and (b) between model and simulation corresponds to a variable offset in the solid conductivity. Hence, a correction term appears to be needed in the theoretical prediction $k_{0,th} = \frac{1}{4}k_{fib}\pi d^2\langle n_z\rangle\langle|\cos\theta|\rangle$ to accurately describe fibrous media with low a or V_f . Contrary to fiber orientation, these two parameters are found to have a significant effect on the average number of contacts per fiber $\langle N_c\rangle$, indicating the accordance with the model from Zhao et al. [48] and Volkov and Zhigilei [46] may be determined by the degree of connectivity of the simulated network. Indeed, when the aspect ratio or the density is low, the connectivity is low and the correlations between fiber temperatures may become non-negligible [47]. To validate this hypothesis, a modified version of the theoretical framework is derived in Appendix B, taking into account the contributions of correlations. This new model results in the following expression for the solid conductivity:

$$k_{cond,solid} = k_{0,th}h\frac{1}{1+r} \quad (5)$$

with

$$h = 1 + \frac{\langle\delta T_{ij}\rangle}{\nabla T_z\langle H\rangle} \quad (6)$$

where $\langle\delta T_{ij}\rangle$ represents the average contribution of correlations in the temperature difference at junctions, and $\nabla T_z = \Delta T/L$ is the global temperature gradient imposed in the sample.

According to this modified model, the predicted conductivity at any contact resistance is modified by a factor h compared with the initial model; its accuracy is evaluated in Fig. 10. In this graph, the colored symbols show $k_0/k_{0,th}$, the ratio of the simulated conductivity at $R_k = 0$ to its corresponding estimation by the initial model, as a function of $\langle N_c\rangle$. Note that this data corresponds to that of Fig. 8(a) and (b) obtained for different aspect ratios and volume fractions. It shows that the evolution of $k_0/k_{0,th}$ can be described by a single curve that depends only on $\langle N_c\rangle$, independently of the values of a and V_f . This finding confirms that the observed reduction in the simulated conductivity compared with that predicted by the initial model is driven by network connectivity, accurately quantified by the average number of contacts per fiber. It can be qualitatively explained by the fact that in a highly-connected network, almost all fibers contribute to heat transfer, whereas only a small proportion of them do so in a poorly-connected one. Furthermore, grey symbols in Fig. 10 represent estimations of h obtained by Eq. (6), for different aspect ratios and densities as well. Calculating h only necessitates the additional measurement of $\langle\delta T_{ij}\rangle$ in simulations. This is achieved using the following expression extracted from

the derivation of the modified theoretical model (see Appendix B):

$$\langle\delta T_{ij}\rangle = \langle|\Delta T_{ij}|\rangle - \langle H\rangle\left(\nabla T_z - \left\langle\frac{dT}{dz}\right\rangle\right) \quad (7)$$

where $\langle|\Delta T_{ij}|\rangle$ is the average temperature difference between two fibers at a junction, and $\langle\frac{dT}{dz}\rangle$ is the average temperature gradient in fibers along the z -direction. The quantity h should correspond to the corrective prefactor $k_0/k_{0,th}$ needed to account for low-connectivity networks. Fig. 10 shows good agreement between these two quantities, despite notable fluctuations in the calculated values of h . Note that finding $0 \leq h \leq 1$ is a direct result of $\langle\delta T_{ij}\rangle$ being a negative value, indicating temperature differences at junctions are lower in average in the modified model. Indeed, considering the correlations results in a reduction of temperature differences between closely positioned fibers, especially those in direct contact. A deviation is observed at high $\langle N_c\rangle$, with $k_0/k_{0,th}$ reaching values higher than 1. As the connectivity increases, the prefactor of the theoretical model should tend towards 1: this suggests that $k_0/k_{0,th}$ may be slightly overestimated by our simulations, while the estimate for h appears to have rectified this discrepancy, indicating a higher level of accuracy. The dashed line plotted in Fig. 10 represents the best fit of the numerical data obtained for h by a rational function $h = C_1\frac{\langle N_c\rangle - C_2}{\langle N_c\rangle - C_3}$ where C_1 , C_2 and C_3 are adjustable parameters; the choice of such a function being motivated by the form of Eq. (6). This best fit gives $C_1 \approx C_3 \approx 1$ and $C_2 \approx 2.18$, confirming our data is consistent with $h \rightarrow 1$ when $\langle N_c\rangle \rightarrow \infty$. The obtained

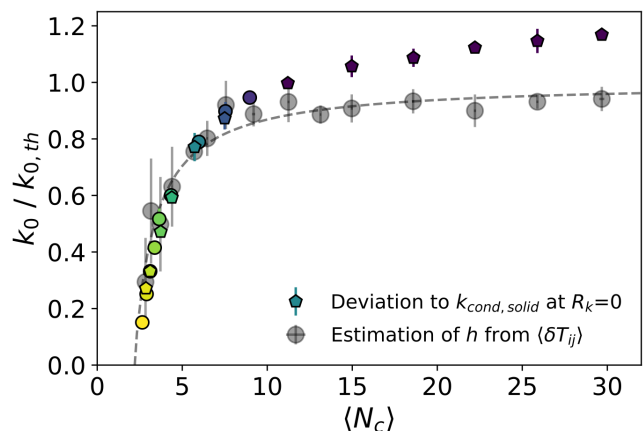


FIG. 10. Ratio of k_0 , the simulated conductivity at $R_k = 0$, to $k_{0,th}$, its corresponding theoretical prediction by the initial model according to Eq. (4), as a function of the average number of contacts per fiber $\langle N_c\rangle$. Colored symbols correspond to simulation results presented in Fig. 8(a) and 8(b), i.e., with different aspect ratios and volume fractions. The grey markers and the associated dashed curve represent the predictions of h calculated from Eqs. (6) and (7).

best fit function can be rewritten as:

$$h = 1 - \frac{\langle N_c \rangle_l - 1}{\langle N_c \rangle - 1} \quad (8)$$

where $\langle N_c \rangle_l = C_2 = 2.18$ is the minimum number of contacts per fiber ensuring a conductive network, i.e., that corresponds to the percolation threshold. Note that as the minimum number of contacts for each fiber is 2 to form a fully-connected network where thermal transfers can be solved, it was expected that the minimum value averaged at the network scale would indeed be slightly higher. In previous studies [46, 60], the average number of contacts per fiber has been expressed as a function of the input parameters: for 3D networks, $\langle N_c \rangle = 2aV_f$. Therefore, Fig. 10 can be interpreted as demonstrating a percolative behavior for 3D networks governed by both volume fraction and aspect ratio: in particular, when a approaches 0, regardless of the value of V_f , the network conductivity becomes zero, as it falls below the percolation threshold. As stated in Ref. [49], this constitutes a major difference with 2D networks, for which the conductivity can remain finite for very small aspect ratios: this is due to the topological difference between 2D and 3D networks.

$\langle N_c \rangle - 1$ can be interpreted as the average number of conducting segments per fiber, each one of them being delimited by contact points. Therefore, the deviation from unity of h , which is due to the correlation term $\frac{\langle \delta T_{ij} \rangle}{\nabla T_z \langle H \rangle}$ according to Eq. (6), can be entirely explained by this number of segments per fiber. As it decreases and approaches its percolation limit value, temperature distributions along fibers exhibit more pronounced piecewise-linear behavior, therefore increasingly deviating from a linear gradient, as it can be seen in Fig. S4 (Supplementary Material) [50]. This explains the growing importance of the impact of correlations in the approximate decomposition of the temperature of a fiber made in the theoretical model (see Eq. (B4) in Appendix B). More generally, this result shows that the solid conductivity in any 3D network of straight fibers can be predicted based on geometric considerations only, using Eqs. (5) and (8), which do not require the resolution of the heat transfer problem.

Eq. (8) also allows to compute a threshold value for $\langle N_c \rangle$, above which the initial model from Zhao et al. [48] and Volkov and Zhigilei [46] can be considered as sufficient. For a 5% tolerance, this threshold is $\langle N_c \rangle_{t,5\%} = 24.6$. This value may be seen as a separation between two characteristic connectivity regimes for a 3D fibrous assembly, generalizing the low-density and high-density regimes described in section III A 1, where we gave a rough estimate for a given case with fixed fiber dimensions. In addition, the expression introduced previously linking the average number of contacts per fiber to the network input parameters in 3D networks, $\langle N_c \rangle = 2aV_f$, can be used to estimate before any numerical generation the value of h for a given set of network parameters. For

an average aspect ratio $a = 100$, representative of fibers in glasswool, the threshold $\langle N_c \rangle_{t,5\%} = 24.6$ converts into a minimum volume fraction $V_{f,t,5\%} = 0.123$. This result indicates that to accurately represent most of glasswool insulation mats, that exhibit lower densities, the model taking into account correlations that we derived and validated in this study should be considered, underlining the interest of this work.

In practice, to predict the thermal conductivity of a specific fibrous insulation material using this model, according to Eqs. (5) and (8), the input parameters d , l , $\langle \cos \theta \rangle$, V_f , R_k and k_f must be known. The three additional quantities $\langle N_c \rangle$, $\langle H \rangle$ and $\langle n_z \rangle$ necessary to calculate $k_{cond,solid}$ can then be obtained from the numerical generation of a fibrous network characterized by the above parameters, as it is done in this study. For example, Fig. 11 compares our results for $k_{cond,solid}$ calculated by simulations and by this theoretical approach based on morphological parameters only, using as input parameters $d = 10 \mu\text{m}$, $l = 1 \text{ mm}$, $\theta = 79.9^\circ$, and $k_f = 1.3 \text{ W}\cdot\text{m}^{-1}\cdot\text{K}^{-1}$, considered as mentioned before as relevant average values when considering glasswool. The selected volume fractions, lower than 0.025, typically represent real-world samples, exhibiting densities lower than $60 \text{ kg}\cdot\text{m}^{-3}$. For each fiber volume fraction, the corresponding material density is estimated from glass density $\rho_{glass} = 2200 \text{ kg}\cdot\text{m}^{-3}$ and taking into account the presence of an organic binder in which the fibers are embedded, with a density twice lower than that of glass and which represents around 10% of the total solid vol-

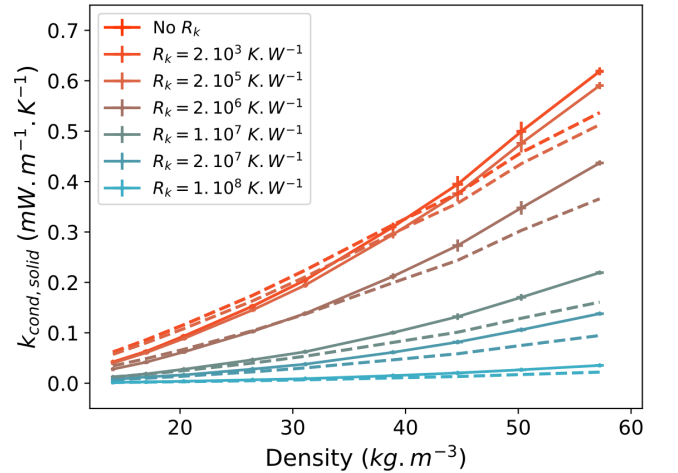


FIG. 11. Simulated (plain line) and theoretically estimated (dashed line) solid conductivity as a function of estimated glasswool density, calculated based on fiber volume fraction and considering the additional presence of binder in real samples. The constant input parameters are $l = 1 \text{ mm}$, $d = 10 \mu\text{m}$ and $\theta = 79.9^\circ$, with fiber volume fractions V_f ranging from 0.006 to 0.03. The solid conductivities estimated using the theoretical model presented above are obtained using Eqs. (5) and (8).

ume [53]. The values of fiber-to-fiber contact resistances R_k , which are not precisely known in real samples, are picked within a probable range, set from 0 to 10^8 KW^{-1} . Previous studies have indeed estimated the contact resistance between two glass fibers with a diameter of $10 \mu\text{m}$ to be of the order of 10^7 KW^{-1} [62–64], and it is likely that the binder can only reduce this resistance, by allowing larger contact areas. Fig. 11 indicates that the solid conductivity for glasswool densities ranging from 10 to 60 kg.m^{-3} would be lower than $0.7 \text{ mW.m}^{-1}.\text{K}^{-1}$. In the density range studied here, a contact resistance $R_k = 10^7 \text{ KW}^{-1}$ would approximately lead to a 55 to 70% decrease in $k_{cond,solid}$ compared with the case of infinitely conductive contacts; this impact of contacts tends to increase when the density decreases, as already demonstrated in section III A 1. According to Fig. 11, predicting $k_{cond,solid}$ using the theoretical approach based on the numerical generation of fibrous networks leads to a 13% maximum relative deviation with simulation results. An alternative for the prediction of solid conductivity with the theoretical model could also be to measure the needed geometric parameters in reconstructed structures from X-ray tomography images, such as those studied in Ref. [7] in the case of glasswool, and to inject them in Eqs. (5) and (8). Note that this theoretical model has been derived for constant values of input parameters, hence the need to consider average values when applying it to the prediction of solid conductivity of real-world insulation materials.

Experimentally, the thermal performance of insulation materials in the steady-state is usually measured using the guarded hot plate method (ISO 8302) or the heat-flux meter method (ISO 8301): the heat flux going through the material is measured when it is placed between two plates at different temperatures, and the effective conductivity is obtained by Fourier’s law. As stated in the introduction, radiation and conduction through gas also affect this quantity and cannot be overlooked in this kind of experiment. To validate our modeling results, a crude approach could be to compare the simulated solid conductivity with an estimate derived from measurements of the effective conductivity, after subtracting predicted contributions of radiation and gaseous conduction. Langlais and Klarsfeld have previously estimated the effective conductivity for low densities typical of glasswool mats, between 10 and 60 kg.m^{-3} , to be of the order of $30\text{--}45 \text{ mW.m}^{-1}.\text{K}^{-1}$ [1]. The effective conductivity is measured with an uncertainty of $\pm 3\%$ as requested by ISO standards: this results in a confidence interval covering approximately 1.8 to $2.7 \text{ mW.m}^{-1}.\text{K}^{-1}$, which could be even broadened considering the challenging aspects of accurately predicting the radiative contribution, that depends on the structure of the material and on the levels of temperature involved [65]. Fig. 11 indicates that when considering input parameters representative of those of glasswool, the simulated solid conductivity is below $0.7 \text{ mW.m}^{-1}.\text{K}^{-1}$. Given this relatively small contribution compared with the uncertainty levels asso-

ciated with the proposed experimental evaluation procedure, one can only state that the order of magnitude of $k_{cond,solid}$ predicted by our model is consistent with the measured value of the effective conductivity of glasswool mats. Only cryogenic experiments in vacuum aimed at suppressing the contributions of conduction and radiation would allow a proper validation of solid conductivity predictions.

IV. CONCLUSION

In summary, we have numerically generated 3D networks representative of fibrous insulation materials such as glasswool, and we have developed an original and efficient nodal simulation approach to analyze their steady-state solid thermal conductivity, integrating the effect of fiber-to-fiber thermal contact resistances. We have investigated the effects of fiber length, diameter, volume fraction and angle, and we have demonstrated that the evolution of solid conductivity in 3D networks is governed by a master curve that depends on a characteristic ratio of thermal resistances, which is an innovative way of describing the behavior of this quantity. This approach also constitutes an exhaustive validation in the 3D case of the underlying theoretical model, which had previously been numerically validated in the specific case of 2D carbon nanotube networks [46–48]; a first comparison with 3D simulation results having been presented only very recently [49], but for more limited ranges of fiber geometric parameters. In particular, a distinction of this present work is the consideration of various fiber orientations, i.e., the investigation of anisotropic systems, which is particularly important when considering insulation materials like glasswool. In this material, fibers also exhibit relatively low aspect ratios and low densities: we have shown that in these cases, a modified theoretical model is required to take into account the influence of correlations between fiber temperatures. We have in particular introduced a simple form of this new model, applicable to a wide range of fibrous materials, highlighting the significance of the average number of contacts per fiber as a key geometric parameter to describe the degree of connectivity of the networks. This model, which enables predictions of solid conductivity based solely on morphological parameters, represents a significant advancement in enhancing the accuracy of thermal performance predictions for insulation materials.

All the conclusions drawn in this study also apply to the prediction of the electrical conductivity of 3D fibrous materials due to the thermal-electric analogy [66]. Therefore, this work paves the way for further investigating the conduction of heat or electricity through the solid structure in fibrous materials with more complex properties. We plan to extend the use of the nodal method to assemblies of non-straight fibers, which could be generated using an approach similar to that of Kallel et al. [27]. A lower solid conductivity is expected when introducing

fiber curviness, as the effective length between the ends of fibers will be reduced, thus decreasing the number of conduction paths [40, 67]. For a more accurate representation of real fibrous samples, the variability of fiber parameters in real samples should also be accounted for, using distributions in the model, as well as the correlations existing between them. The presumed link between contact resistance and fiber diameter was indeed already discussed as an interesting next inclusion in the model, but the link between fiber length and diameter could also be explored. Finally, we plan to integrate in the model presented here the results of future experimental measurements of contact resistance between two glass fibers, in order to provide insight about the extent of the impact of contacts in real glasswool samples.

ACKNOWLEDGMENTS

The authors are grateful to Jean-Marie Chassot (Institut Langevin) who recorded the optical coherence tomography image of a glasswool mat shown in the supplementary material, using LLTech commercial system. This work pertains to the French government program "France2030" (EUR INTREE and LABEX INTERACTIFS). This work is supported by the ANRT (Association nationale de la recherche et de la technologie) thanks to a CIFRE fellowship granted to C. Gaunand. This work was also supported by the "Investissements d'Avenir" program launched by the French Government (Labex WiFi).

Appendix A: Resolution of the linear thermal circuit system using a nodal method

In the steady-state configuration considered in this study, the thermal network can be described by two matrices: the incidence matrix and the conductance matrix. They respectively account for the two factors affecting the overall conductivity: the network structure and the material properties [32].

The incidence matrix of a graph with n nodes and m branches $\mathbf{A} = (a_{fg})_{1 \leq f \leq m, 1 \leq g \leq n}$ is defined by [68]:

$$a_{fg} = \begin{cases} 0 & \text{if the branch } f \text{ is not connected to the node } g \\ +1 & \text{if the flow through the branch } f \text{ enters the node } g \\ -1 & \text{if the flow through the branch } f \text{ leaves the node } g. \end{cases} \quad (\text{A1})$$

The rows of the matrix \mathbf{A} correspond to the branches, and the columns correspond to the nodes. As the heat fluxes through branches have defined directions, the network is a directed graph, hence an oriented incidence matrix.

The conductance matrix $\mathbf{G} = (g_{fh})_{1 \leq f, h \leq m}$ is diagonal

and is of dimension equal to the number of branches m :

$$g_{fh} = \begin{cases} R_f^{-1} & \text{if } f = h \\ 0 & \text{if } f \neq h \end{cases} \quad (\text{A2})$$

where R_f is the thermal resistance associated with the branch f . If the branch represents a fiber, its resistance is an internal resistance: $R_f = \frac{4l_f}{k_{fib}\pi d^2}$ where l_f is the length of the branch (i.e., the distance between the two associated nodes). If it represents a contact, its resistance is a contact resistance: $R_f = R_k$ where R_k is a value we impose for all contacts in the assembly. The introduction of the contact resistance as an effective value is chosen due to the soft-core approach used in this numerical model: there is no dependence on the individual properties of the contacts.

The thermal network has to be solved to access two vectors: the vector of temperatures \mathbf{t} , of size equal to the number of nodes n , and that of heat fluxes \mathbf{q} , of size equal to the number of branches m .

For any branch f , the temperature drop is $e_f = t_{g-1} - t_g + b_f$, where t_g and t_{g-1} are the temperatures of the connected nodes and b_f the possible temperature source term. The heat flux through the branch is linked to this temperature difference and to the thermal resistance associated to the branch by the Fourier's Law: $q_f = e_f/R_f$. Expressed for all branches in matrix form, these two equations become:

$$\mathbf{e} = -\mathbf{A}\mathbf{t} + \mathbf{b} \quad (\text{A3})$$

and

$$\mathbf{q} = \mathbf{G}\mathbf{e} \quad (\text{A4})$$

where \mathbf{e} is the m -dimensional vector of temperature drops over the thermal resistances. Combining Eqs. (A3) and (A4) gives:

$$\mathbf{G}^{-1}\mathbf{q} + \mathbf{A}\mathbf{t} = \mathbf{b} \quad (\text{A5})$$

where \mathbf{b} is the m -dimensional of temperature sources.

For any node g , the balance of heat rates can be expressed as $\sum_g q_g + s_g = 0$, where $\sum_g q_g$ is the algebraic sum of heat fluxes entering the node and s_g is a possible heat flow source. Expressed for all nodes in matrix form, this equation becomes:

$$-\mathbf{A}^T\mathbf{q} = \mathbf{s} \quad (\text{A6})$$

where \mathbf{A}^T is the transpose of the incidence matrix, and \mathbf{s} is the n -dimensional vector of heat flow sources.

Combining the two constitutive equations for conductive heat transfer (A5) and (A6), we obtain:

$$\mathbf{0} = -\mathbf{A}^T\mathbf{G}\mathbf{A}\mathbf{t} + \mathbf{A}^T\mathbf{G}\mathbf{b} + \mathbf{s}. \quad (\text{A7})$$

In the network configuration described above, there is no heat flux source (i.e., $\mathbf{s} = \mathbf{0}$), only temperature sources at the top and bottom nodes: they are associated to the corresponding branches, to include them in the vector \mathbf{b} . Eq. (A7) is solved in order to get the vector of temperatures and that of heat fluxes.

Appendix B: Derivation of the low-connectivity model for solid conduction in fibrous networks

This model is built on a similar basis than that introduced by Volkov and Zhigilei [46] and Zhao et al. [48] for 2D and 3D dense networks, and that presented later by Volkov and Zhigilei [47] for 2D semi-dilute networks. In this proposed version, a corrective prefactor is introduced to accurately represent 3D fibrous networks with low connectivity, i.e., low density or low aspect ratio. In this case, the temperature gradients in the fibers can vary significantly, largely influenced by their proximity to other fibers.

In the guarded hot plate configuration, Fourier's law gives the steady state heat flux in the vertical direction Q as a function of the thermal conductivity of the material, the established temperature gradient in the vertical direction ∇T_z , and the horizontal cross-sectional area $A_z = L^2$. As the thermal conductivity only accounts for conduction through the solid phase, Fourier's law directly gives the solid conductivity: $Q = -k_{cond,solid} A_z \nabla T_z$. This also implies that Q is the algebraic sum of all heat flows through the fibers that cross the section A_z , which means that it can be expressed by an averaging approach: $Q = -A_z \langle n_z \rangle \langle Q_i \rangle$ where $\langle Q_i \rangle$ is the average flux crossing one fiber (with $Q_i \geq 0$ if heat flows in the fiber from the end closer to the hot plate to the other end; this fiber direction will be referred to as w_i), and $\langle n_z \rangle$ is the average areal number density of fibers through a horizontal section. Note that $\langle Q_i \rangle \geq 0$ on average, which makes Q a negative quantity, consistently with the coordinate system chosen in Fig. 1(a) and as represented in Fig. 3. The solid conductivity can therefore be given by:

$$k_{cond,solid} = \frac{\langle n_z \rangle \langle Q_i \rangle}{\nabla T_z}. \quad (\text{B1})$$

At the fiber scale, the flux Q_i can be expressed by a local Fourier's law: $Q_i = -k_{fib} A_{fib} \frac{dT_i}{dw_i}$ with $\frac{dT_i}{dw_i}$ the temperature gradient in the direction w_i of the fiber i , k_{fib} the intrinsic fiber conductivity and $A_{fib} = \pi d^2/4$ the fiber cross-section. The conductivity and the cross-section being held constant for all fibers in the network, an average form can be written as follows:

$$\langle Q_i \rangle = -k_{fib} A_{fib} \left\langle \frac{dT_i}{dw_i} \right\rangle. \quad (\text{B2})$$

This approach relies on the assumption of a constant average temperature gradient, that takes into account the

contribution of fibers conveying heat flux in the opposite direction to the global steady-state heat flux established in the sample. Introducing the average cosine of the polar angle θ , this temperature gradient can be expressed along the z -direction by:

$$\left\langle \frac{dT}{dz} \right\rangle = \frac{-\langle \frac{dT_i}{dw_i} \rangle}{\langle |\cos \theta| \rangle}. \quad (\text{B3})$$

Hence, the temperature of fiber i at a given z -coordinate is given by the following decomposition:

$$T_i(z) = T_b + \nabla T_z z_{c_i} + \left\langle \frac{dT}{dz} \right\rangle (z - z_{c_i}) + \delta T_i(z) \quad (\text{B4})$$

where T_b is the source temperature at $z = 0$, z_{c_i} is the z -coordinate of the center of the fiber, and δT_i is a corrective term accounting for the deviation of the real temperature distribution along fiber i from the linear one. In particular, this term can represent the contribution of correlations existing between the temperatures of two fibers in contact. For two fibers i and j in contact, at $z = z_{ij}$ (the position of the contact on fiber i) and $z = z_{ji}$ (the position of the contact on fiber j), respectively, Eq. (B4) gives:

$$T_i(z_{ij}) = T_b + \nabla T_z z_{c_i} + \left\langle \frac{dT}{dz} \right\rangle (z_{ij} - z_{c_i}) + \delta T_i(z_{ij})$$

and

$$T_j(z_{ji}) = T_b + \nabla T_z z_{c_j} + \left\langle \frac{dT}{dz} \right\rangle (z_{ji} - z_{c_j}) + \delta T_j(z_{ji}).$$

As the values chosen in this study for fiber diameter, that acts as the distance threshold for contact detection, are about two orders of magnitude smaller than fiber length, it is reasonable to assume that $z_{ij} \approx z_{ji}$. Then, the temperature difference at a junction is given by:

$$\begin{aligned} \Delta T_{ij} &= T_j(z_{ji}) - T_i(z_{ij}) \\ &= \left(\nabla T_z - \left\langle \frac{dT}{dz} \right\rangle \right) (z_{c_j} - z_{c_i}) + \delta T_{ij} \end{aligned} \quad (\text{B5})$$

where $\delta T_{ij} = \delta T_j(z_{ji}) - \delta T_i(z_{ij})$ represents the correction on the estimated temperature drop due to correlations. Considering heat transfer will occur from the fiber whose center is closer to the hot plate to the other one, and introducing $\langle H \rangle = |z_{c_j} - z_{c_i}|$ the average z -distance between two fibers in contact, averaging Eq. (B5) results in:

$$\langle |\Delta T_{ij}| \rangle = \langle H \rangle \left(\nabla T_z - \left\langle \frac{dT}{dz} \right\rangle \right) + \langle \delta T_{ij} \rangle. \quad (\text{B6})$$

On average, one can assume that the flux through one fiber $\langle Q_i \rangle$ flows in or out through half of the contacts, as each contact corresponds to two fibers: $\langle Q_i \rangle = \langle \frac{1}{2} \sum_j |Q_{ij}| \rangle$, where $|Q_{ij}|$ is the net interface flux between fibers i and j , governed by the value of the contact resistance: $|Q_{ij}| = \frac{|T_j - T_i|}{R_k}$. This flow balance can be therefore written as:

$$\langle Q_i \rangle = \frac{\langle N_c \rangle \langle |\Delta T_{ij}| \rangle}{2R_k} \quad (\text{B7})$$

where $\langle N_c \rangle$ is the average number of contacts per fiber. Using Eqs. (B2), (B3) and (B7), the following relationship between the average temperature gradient along fibers in the z -direction and the average temperature drop at a junction is obtained:

$$\left\langle \frac{dT}{dz} \right\rangle = \frac{\langle Q_i \rangle}{\langle |\cos \theta| \rangle k_{fib} A_{fib}} = \frac{\langle N_c \rangle \langle |\Delta T_{ij}| \rangle}{2R_k \langle |\cos \theta| \rangle k_{fib} A_{fib}}. \quad (\text{B8})$$

By substituting Eq. (B8) into Eq. (B6), one can find the following expression for the average temperature drop at junctions:

$$\langle |\Delta T_{ij}| \rangle = \nabla T_z \langle H \rangle \frac{1 + \frac{\langle \delta T_{ij} \rangle}{\nabla T_z \langle H \rangle}}{1 + \frac{\langle H \rangle \langle N_c \rangle}{2R_k \langle |\cos \theta| \rangle k_{fib} A_{fib}}}. \quad (\text{B9})$$

Combining Eq. (B1) and Eq. (B7), we have: $k_{cond,solid} = \frac{\langle n_z \rangle \langle N_c \rangle \langle |\Delta T_{ij}| \rangle}{2R_k \nabla T_z}$. This expression for the solid conductivity can be inserted in Eq. (B9), which gives its evolution as a function of ∇T_z , $\langle \delta T_{ij} \rangle$ and the geometric parameters of the network:

$$k_{cond,solid} = k_{fib} A_{fib} \langle n_z \rangle \langle |\cos \theta| \rangle \left(1 + \frac{\langle \delta T_{ij} \rangle}{\nabla T_z \langle H \rangle} \right) \times \frac{1}{1 + \frac{2R_k \langle |\cos \theta| \rangle k_{fib} A_{fib}}{\langle H \rangle \langle N_c \rangle}}. \quad (\text{B10})$$

Using the notations introduced in section III B, $r = \frac{2l \langle |\cos \theta| \rangle R_k}{\langle H \rangle \langle N_c \rangle R_{fib}} = \frac{2R_k \langle |\cos \theta| \rangle k_{fib} A_{fib}}{\langle H \rangle \langle N_c \rangle}$ and $k_{0,th} = k_{fib} A_{fib} \langle n_z \rangle \langle |\cos \theta| \rangle$, Eq. (B10) can be written as:

$$k_{cond,solid} = \left(1 + \frac{\langle \delta T_{ij} \rangle}{\nabla T_z \langle H \rangle} \right) k_{0,th} \frac{1}{1+r}. \quad (\text{B11})$$

-
- [1] C. Langlais and S. Klarsfeld, Isolation thermique à température ambiante. Transferts de chaleur, Techniques de l'Ingénieur - Énergies - Thermique pour l'industrie, BE9859 (2004).
- [2] C. Bankvall, *Heat transfer in fibrous materials*, Vol. D4 (Byggeforskningsrådet (BFR), 1972).
- [3] T. Tong and C. Tien, Analytical Models for Thermal Radiation in Fibrous Insulations, *Journal of Thermal Insulation* **4**, 27 (1980).
- [4] D. Baillis and J.-F. Sacadura, Thermal radiation properties of dispersed media: theoretical prediction and experimental characterization, *Journal of Quantitative Spectroscopy and Radiative Transfer* **67**, 327 (2000).
- [5] R. Arambakam, H. V. Tafreshi, and B. Pourdeyhimi, Dual-scale 3-D approach for modeling radiative heat transfer in fibrous insulations, *International Journal of Heat and Mass Transfer* **64**, 1109 (2013).
- [6] J. Randrianalisoa, S. Haussener, D. Baillis, and W. Lipiński, Radiative characterization of random fibrous media with long cylindrical fibers: Comparison of single- and multi-RTE approaches, *Journal of Quantitative Spectroscopy and Radiative Transfer* **202**, 220 (2017).
- [7] R. Meftah, S. Berger, G. Jacqus, J.-Y. Lалуé, and V. Cnudde, Multiscale characterization of glass wools using X-ray micro-CT, *Materials Characterization* **156**, 109852 (2019).
- [8] M. Faessel, C. Delisée, F. Bos, and P. Castéra, 3D Modelling of random cellulosic fibrous networks based on X-ray tomography and image analysis, *Composites Science and Technology* **65**, 1931 (2005).
- [9] F. Panerai, J. C. Ferguson, J. Lachaud, A. Martin, M. J. Gasch, and N. N. Mansour, Micro-tomography based analysis of thermal conductivity, diffusivity and oxidation behavior of rigid and flexible fibrous insulators, *International Journal of Heat and Mass Transfer* **108**, 801 (2017).
- [10] X. Huang, Q. Zhou, J. Liu, Y. Zhao, W. Zhou, and D. Deng, 3D stochastic modeling, simulation and analysis of effective thermal conductivity in fibrous media, *Powder Technology* **320**, 397 (2017).
- [11] P. Townsend, E. Larsson, T. Karlson, S. A. Hall, M. Lundman, P. Bergström, C. Hanson, N. Lorén, T. Gebäck, A. Särkkä, and M. Röding, Stochastic modelling of 3D fiber structures imaged with X-ray microtomography, *Computational Materials Science* **194**, 110433 (2021).
- [12] B. Pourdeyhimi, B. Mazé, and H. V. Tafreshi, Simulation and Analysis of Unbonded Nonwoven Fibrous Structures, *Journal of Engineered Fibers and Fabrics* **1** (2006).
- [13] N. Provatás, M. Haataja, E. Seppälä, S. Majaniemi, J. Åström, M. Alava, and T. Ala-Nissila, Growth, percolation, and correlations in disordered fiber networks, *J Stat Phys* **87**, 385 (1997).
- [14] A. Kulachenko and T. Uesaka, Direct simulations of fiber network deformation and failure, *Mechanics of Materials* **51** (2012).
- [15] D. G. Venkateshan, M. A. Tahir, H. Vahedi Tafreshi, and B. Pourdeyhimi, Modeling effects of fiber rigidity on thickness and porosity of virtual electrospun mats, *Materials & Design* **96**, 27 (2016).
- [16] A. Naddeo and N. Cappetti, Automatic versatile parametric procedure for a complete FEM structural analysis of composites having cylinder-shaped reinforcing fibres, *Computational Materials Science* (2014).
- [17] C. Redenbach and I. Vecchio, Statistical analysis and stochastic modelling of fibre composites, *Composites Science and Technology* **71**, 107 (2011).
- [18] G. Matheron, *Random sets and integral geometry*, Wiley series in probability and mathematical statistics (J. Wiley & Sons, 1975).
- [19] J. Ohser and K. Schladitz, Model-Based Image Analysis, in *3D Images of Materials Structures* (John Wiley & Sons, Ltd, 2009) pp. 233–280.
- [20] G. Gaiselmann, D. Froning, C. Tötze, C. Quick, I. Manke, W. Lehnert, and V. Schmidt, Stochastic 3D modeling of non-woven materials with wet-proofing agent, *International Journal of Hydrogen Energy* **38**,

- 8448 (2013).
- [21] H. Altendorf and D. Jeulin, Random Walk Based Stochastic Modeling of 3D Fiber Systems, *Physical Review E : Statistical, Nonlinear, and Soft Matter Physics* **83**, 10 p., 041804 (2010).
- [22] L. Chapelle, M. Lévesque, P. Brøndsted, M. R. Foldschack, and Y. Kusano, Generation of non-overlapping fiber architecture: 20th International Conference on Composite Materials, Proceedings of the 20th International Conference on Composite Materials (2015).
- [23] S. Abishek, A. J. C. King, R. Mead-Hunter, V. Golkarfard, W. Heikamp, and B. J. Mullins, Generation and validation of virtual nonwoven, foam and knitted filter (separator/coalescer) geometries for CFD simulations, *Separation and Purification Technology* **188**, 493 (2017).
- [24] M. Foygel, R. D. Morris, D. Anez, S. French, and V. L. Sobolev, Theoretical and computational studies of carbon nanotube composites and suspensions: Electrical and thermal conductivity, *Phys. Rev. B* **71**, 104201 (2005).
- [25] Q. Wang, Correlations in Hard- and Soft-Core Generic Polymer Models, *Polymers (Basel)* **15**, 1180 (2023).
- [26] R. Arambakam, H. Vahedi Tafreshi, and B. Pourdeyhimi, A simple simulation method for designing fibrous insulation materials, *Materials & Design* **44**, 99 (2013).
- [27] H. Kallel and K. Joulain, Design and thermal conductivity of 3D artificial cross-linked random fiber networks, *Materials & Design* **220**, 110800 (2022).
- [28] K. Schladitz, S. Peters, D. Reinel-Bitzer, A. Wiegmann, and J. Ohser, Design of acoustic trim based on geometric modeling and flow simulation for non-woven, *Computational Materials Science* **38**, 56 (2006).
- [29] S. Kirkpatrick, Percolation and Conduction, *Rev. Mod. Phys.* **45**, 574 (1973).
- [30] S. Whitaker, *The Method of Volume Averaging* (Kluwer Academic Publishers, 1999).
- [31] C. G. d. Rocha, H. G. Manning, C. O’Callaghan, C. Ritter, A. T. Bellew, J. J. Boland, and M. S. Ferreira, Ultimate conductivity performance in metallic nanowire networks, *Nanoscale* **7**, 13011 (2015).
- [32] D. Kim and J. Nam, Systematic analysis for electrical conductivity of network of conducting rods by Kirchhoff’s laws and block matrices, *Journal of Applied Physics* **124**, 215104 (2018).
- [33] D. Kim and J. Nam, Analyzing conducting rod networks using centrality, *Electrochimica Acta* **370**, 137725 (2021).
- [34] C. Ghiaus, Causality issue in the heat balance method for calculating the design heating and cooling load, *Energy* **50**, 292 (2013).
- [35] S. Kumar, J. Y. Murthy, and M. A. Alam, Percolating Conduction in Finite Nanotube Networks, *Phys. Rev. Lett.* **95**, 066802 (2005).
- [36] X. Cheng, A. M. Sastry, and B. E. Layton, Transport in Stochastic Fibrous Networks, *Journal of Engineering Materials and Technology* **123**, 12 (2000).
- [37] F. Dalmas, R. Dendievel, L. Chazeau, J.-Y. Cavaillé, and C. Gauthier, Carbon nanotube-filled polymer composites. Numerical simulation of electrical conductivity in three-dimensional entangled fibrous networks, *Acta Materialia* **54**, 2923 (2006).
- [38] M. Žeželj and I. Stanković, From percolating to dense random stick networks: Conductivity model investigation, *Phys. Rev. B* **86**, 134202 (2012).
- [39] A. Behnam and A. Ural, Computational study of geometry-dependent resistivity scaling in single-walled carbon nanotube films, *Phys. Rev. B* **75**, 125432 (2007).
- [40] N. Fata, S. Mishra, Y. Xue, Y. Wang, J. Hicks, and A. Ural, Effect of junction-to-nanowire resistance ratio on the percolation conductivity and critical exponents of nanowire networks, *Journal of Applied Physics* **128**, 124301 (2020).
- [41] F. Incropera, D. Dewitt, T. Bergman, and A. Lavine, *Fundamentals of Heat and Mass Transfer*, 6th ed. (John Wiley & Sons, 2006).
- [42] J.-P. Vassal, L. Orgéas, and D. Favier, Modelling microstructure effects on the conduction in fibrous materials with fibre–fibre interface barriers, *Modelling Simul. Mater. Sci. Eng.* **16**, 035007 (2008).
- [43] A. Kumar and G. U. Kulkarni, Evaluating conducting network based transparent electrodes from geometrical considerations, *Journal of Applied Physics* **119**, 015102 (2016).
- [44] C. Forró, L. Demkó, S. Weydert, J. Vörös, and K. Tybrandt, Predictive Model for the Electrical Transport within Nanowire Networks, *ACS Nano* **12**, 11080 (2018).
- [45] A. Pavlov, D. Mitin, A. Vorobyev, S. Raudik, Y. Berdnikov, A. Mozharov, V. Mikhailovskii, D. V. Krasnikov, D. S. Kopylova, R. Polozkov, A. G. Nasibulin, and I. Mukhin, Conductivity-based approach to estimate average bundle length in randomly oriented network of single-walled carbon nanotubes, *Applied Physics Letters* **123**, 011904 (2023).
- [46] A. N. Volkov and L. V. Zhigilei, Heat conduction in carbon nanotube materials: Strong effect of intrinsic thermal conductivity of carbon nanotubes, *Applied Physics Letters* **101**, 043113 (2012).
- [47] A. N. Volkov and L. V. Zhigilei, Thermal conductivity of two-dimensional disordered fibrous materials defined by interfiber thermal contact conductance and intrinsic conductivity of fibers, *Journal of Applied Physics* **127**, 065102 (2020).
- [48] X. Zhao, C. Huang, Q. Liu, I. I. Smalyukh, and R. Yang, Thermal conductivity model for nanofiber networks, *Journal of Applied Physics* **123**, 085103 (2018).
- [49] A. N. Volkov and L. V. Zhigilei, Thermal Conductivity of Three-Dimensional Disordered Fibrous Materials, preprint available at SSRN: <https://ssrn.com/abstract=4932138> (2024).
- [50] See supplemental material for (1) an optical coherence tomography image of glasswool showing the structure of the material, (2) an illustration of the rve selection procedure, (3) details about the domain sizes used in the simulations presented in this paper, and (4) examples of temperature distributions along fibers in simulated networks.
- [51] H. Altendorf, D. Jeulin, and F. Willot, Influence of the fiber geometry on the macroscopic elastic and thermal properties, *International Journal of Solids and Structures* **51**, 3807 (2014).
- [52] L. Berhan and A. M. Sastry, Modeling percolation in high-aspect-ratio fiber systems. I. Soft-core versus hard-core models, *Phys. Rev. E* **75**, 041120 (2007).
- [53] *Private communication*, Tech. Rep. (Saint-Gobain Recherche Paris, 2024).
- [54] A. Akolkar, N. Rahmatian, S. H. Unterberger, and J. Petrasch, Tomography based analysis of conduction anisotropy in fibrous insulation, *International Journal of Heat and Mass Transfer* **108**, 1740 (2017).

- [55] A. Kaveh, Introduction to Graph Theory and Algebraic Graph Theory, in *Optimal Analysis of Structures by Concepts of Symmetry and Regularity*, edited by A. Kaveh (Vienna, 2013) pp. 15–35.
- [56] L. Chapelle, *Characterization and modelling of the mechanical properties of mineral wool*, Ph.D. thesis, Technical University of Denmark (2016).
- [57] S.-H. Park, J. Hwang, G.-S. Park, J.-H. Ha, M. Zhang, D. Kim, D.-J. Yun, S. Lee, and S. H. Lee, Modeling the electrical resistivity of polymer composites with segregated structures, *Nat Commun* **10**, 2537 (2019).
- [58] A. Kumar, N. S. Vidhyadhiraja, and G. U. Kulkarni, Current distribution in conducting nanowire networks, *Journal of Applied Physics* **122**, 045101 (2017).
- [59] D. Hecht, L. Hu, and G. Gruner, Conductivity scaling with bundle length and diameter in single walled carbon nanotube networks, *Applied Physics Letters* **89**, 133112 (2006).
- [60] T. Komori and K. Makishima, Numbers of Fiber-to-Fiber Contacts in General Fiber Assemblies, *Textile Research Journal* **47**, 13 (1977).
- [61] S. M. Bergin, Y.-H. Chen, A. R. Rathmell, P. Charbonneau, Z.-Y. Li, and B. J. Wiley, The effect of nanowire length and diameter on the properties of transparent, conducting nanowire films, *Nanoscale* **4**, 1996 (2012).
- [62] E. Perros, *Caractérisation locale du transfert de chaleur aux interfaces solide-solide dans les milieux isolants*, Ph.D. thesis, Paris Sciences et Lettres (2017).
- [63] T. D. D. Nguyen, J. Richard, J. Doumouro, Y. De Wilde, and O. Bourgeois, Thermal Exchange of Glass Micro-Fibers Measured by the 3ω Technique, *Journal of Heat Transfer* **142**, 101701 (2020).
- [64] J. Doumouro, E. Perros, A. Dodu, N. Rahbany, D. Lepirat, V. Krachmalnicoff, R. Carminati, W. Poirier, and Y. De Wilde, Quantitative Measurement of the Thermal Contact Resistance between a Glass Microsphere and a Plate, *Phys. Rev. Appl.* **15**, 014063 (2021).
- [65] C. Langlais, G. Guilbert, D. Banner, and S. Klarsfeld, Influence of the Chemical Composition of Glass on Heat Transfer through Glass Fibre Insulations in Relation to Their Morphology and Temperature of Use, *Journal of Thermal Insulation and Building Envelopes* **18**, 350 (1995).
- [66] L. S. Verma, A. K. Shrotriya, R. Singh, and D. R. Chaudhary, Thermal conduction in two-phase materials with spherical and non-spherical inclusions, *J. Phys. D: Appl. Phys.* **24**, 1729 (1991).
- [67] J. Hicks, J. Li, C. Ying, and A. Ural, Effect of nanowire curviness on the percolation resistivity of transparent, conductive metal nanowire networks, *Journal of Applied Physics* **123**, 204309 (2018).
- [68] F. Dörfler, J. W. Simpson-Porco, and F. Bullo, Electrical Networks and Algebraic Graph Theory: Models, Properties, and Applications, *Proceedings of the IEEE* **106**, 977 (2018).

**Supplementary Material for the manuscript:
Modelling conductive thermal transport in three-dimensional
fibrous media with fiber-to-fiber contacts**

Clémence Gaunand

*Institut Langevin, ESPCI Paris, Université PSL, CNRS - Paris (France),
Saint-Gobain Research Paris - Aubervilliers (France) and
Institut Pprime, CNRS, Université de Poitiers,
ISAE-ENSMA - Poitiers (France)*

Yannick De Wilde

Institut Langevin, ESPCI Paris, Université PSL, CNRS - Paris (France),

Adrien François and Veneta Grigorova-Moutiers

Saint-Gobain Research Paris - Aubervilliers (France)

Karl Joulain

*Institut Pprime, CNRS, Université de Poitiers,
ISAE-ENSMA - Poitiers (France)*

(Dated: February 25, 2025)

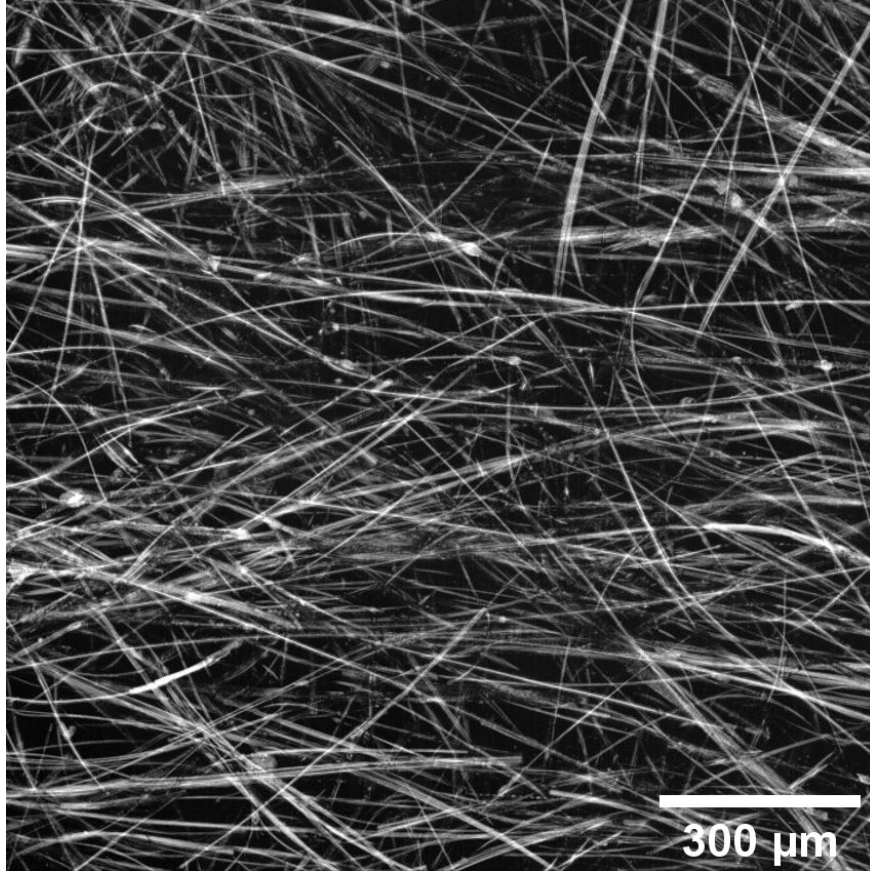


FIG. S1. Optical coherence tomography image of a glasswool mat (top view), with micro-scale resolution, showing the low tortuosity of fibers in this material.

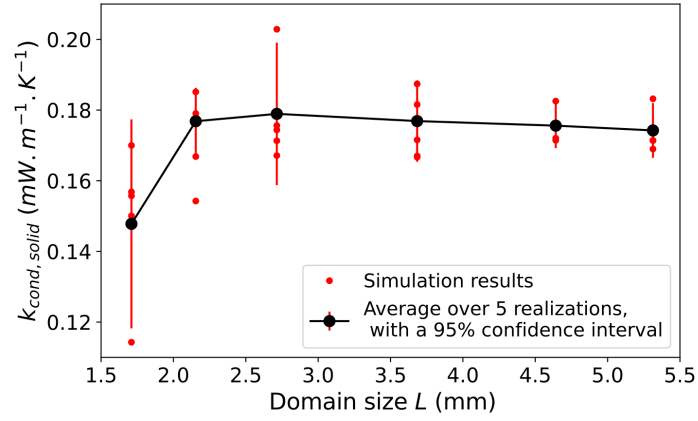


FIG. S2. Illustration of the Representative Volume Element (RVE) selection procedure: for each set of input parameters, the domain size is increased until convergence of the simulation results, which is quantitatively identified by a relative error on the solid thermal conductivity averaged over 5 realizations at a 95% confidence level ϵ_{rel} lower than 5%. In the case shown here, the input parameters are $V_f = 0.01$, $l = 1$ mm, $d = 10$ μm and $\bar{\theta} = 79.9^\circ$, and the RVE determined with this method is 91.125 mm^3 ($L = 4.5$ mm).

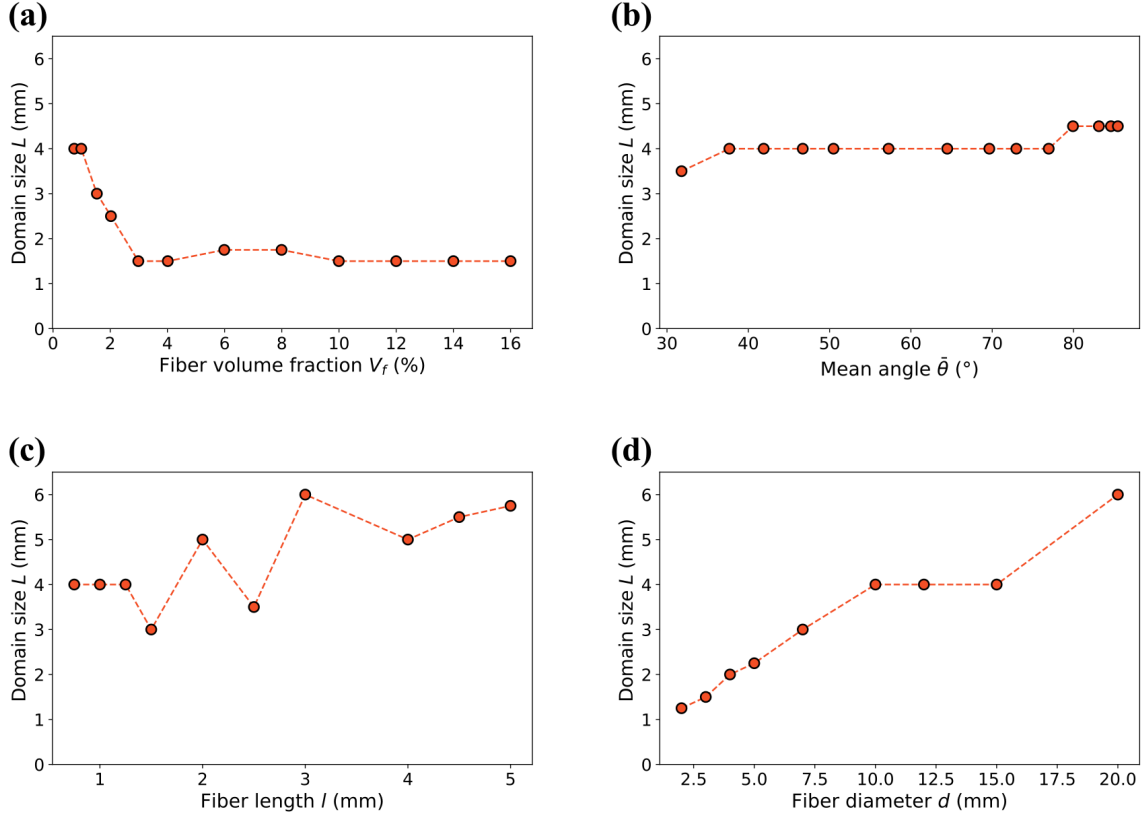


FIG. S3. Domain sizes L used in the simulations presented in this paper, corresponding to a RVE in each case: (a) for different volume fractions, corresponding to data shown in Fig. 4, (b) for different fiber orientations, corresponding to data shown in Fig. 5, (c) for different fiber lengths, corresponding to data shown in Fig. 6, and (d) for different fiber diameters, corresponding to data shown in Fig. 7. The base parameters are $V_f = 0.01$, $\bar{\theta} = 57.3^\circ$, $l = 1$ mm and $d = 10$ μm .

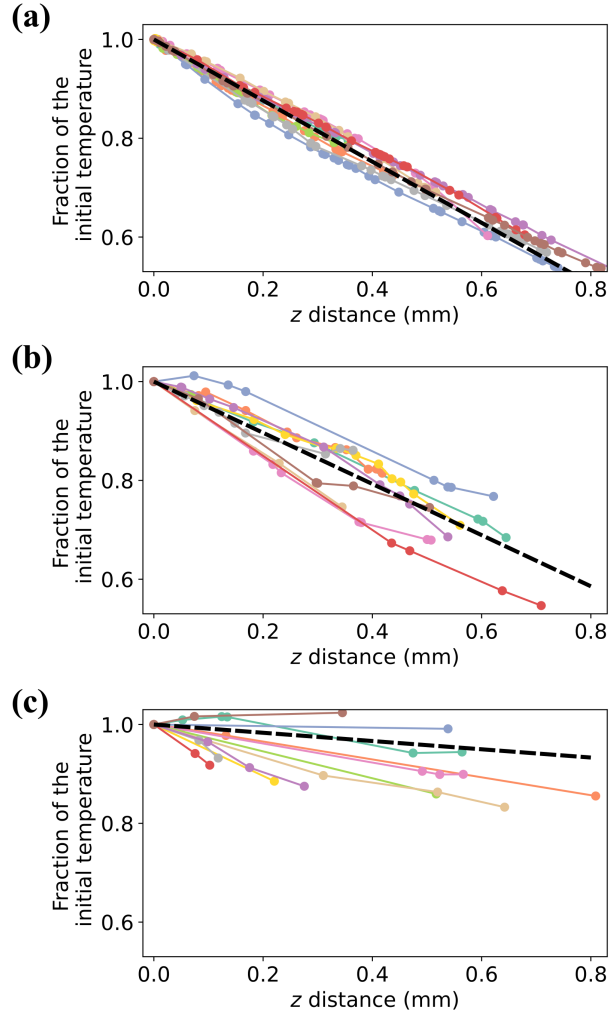


FIG. S4. Temperature distributions along different representative fibers as a function of the vertical position (in color), compared in relative variation to the average linear temperature gradient in fibers in the z direction $\langle \frac{dT}{dz} \rangle$ (slope of the dashed black curve), in networks with (a) $\langle N_c \rangle = 22.2$, (b) $\langle N_c \rangle = 5.7$, and (c) $\langle N_c \rangle = 3.1$.